APPLIED PULSED POWER TECHNOLOGIES
614 1/2 Narcissus Avenue Corona Del Mar, California 92625 (714) 640 5738

April 30, 1997

Final Report

Material Surface Modification Using Pulsed, High Power Plasma-Ion Beam Technology

Submitted to:

Dr. James Hirvonen
Leader, Surface Science Team
U. S. Army Research Laboratory
AMSRL-WM-ME Bldg. 4600
APG, MD 21005-5069

Contract Number: DAAL01-96-C-0075

Submitted by:

Eusebio Garate
Vitaly Bystritskii
Applied Pulsed Power Technologies
614 1/2 Narcissus Avenue
Corona Del Mar, CA 92625

REPORT DOCUMENTATION PAGE

Form Approved
OMB No. 0704-0188

1. AGENCY USE ONLY (*Leave Blank*)	2. REPORT DATE	3. REPORT TYPE AND DATES COVERED
	30APR97	Final Report

4. TITLE AND SUBTITLE

Material Surface Modification Using Pulsed, High Power Plasma-Ion Beam Technology

5. FUNDING NUMBERS

DAAL01-96-C-0075

6. AUTHOR(S)

Eusebio Garate
Vitaly Bystritskii

7. PERFORMING ORGANIZATION NAME(S) AND ADDRESS(ES)

Applied Pulsed Power Technologies
614 1/2 Narcissus Avenue
Corona Del Mar, CA 92625

8. PERFORMING ORGANIZATION REPORT NUMBER

APP0002

9. SPONSORING/MONITORING AGENCY NAME(S) AND ADDRESS(ES)

U.S. Army Research Laboratory
AMSRL-WM-ME Bldg. 4600
APG, MD 21005-5069

10. SPONSORING/MONITORING AGENCY REPORT NUMBER

11. SUPPLEMENTARY NOTES

12a. DISTRIBUTION/AVAILABILITY STATEMENT

Approved for public release; distibution unlimited.

12b. DISTRIBUTION CODE

13. ABSTRACT (*Maximum 200 words*)

Report developed under SBIR contract. The main objective of the Phase I effort was to demonstrate the effectiveness of plasma enhanced, high power, pulsed ion beams, produced in a Microsecond Plasma Opening Switch, for modification of the surface properties of materials. As part of the Phase I work we constructed and tested a system capable of generating an up to 300 keV, 180 A/cm^2 current density, 100 nanosecond ion beam pulse. The plasma enhanced ion beam was used to irradiate various steel and aluminum samples. Measurements indicate that at least a factor of 3 increase in microhardness occurs for the irradiated steel samples. Corrosion resistance, as measured by mass loss and anodic polarization curves, indicates at least a factor of 3 increase in corrosion resistance can be attained for the irradiated aluminum samples. Potential applications include treatment of aircraft aluminum to increase corrosion resistance and treatment of tool steels and other materials to increase hardness and wear resistance.

14. SUBJECT TERMS

SBIR Report Ion Beam Corrosion Resistance Hardness Wear Resistance

15. NUMBER OF PAGES

74

16. PRICE CODE

17. SECURITY CLASSIFICATION OF REPORT	18. SECURITY CLASSIFICATION OF THIS PAGE	19. SECURITY CLASSIFICATION OF ABSTRACT	20. LIMITATION OF ABSTRACT
UNCLASSIFIED	UNCLASSIFIED	UNCLASSIFIED	UL

Abstract

High power ion beam treatment of materials, including carbon steels, stainless steels, aluminum and polymers has resulted in improvements in corrosion and erosion resistance, and microhardness, and has also resulted in microstructural changes of these materials. The main objective of our Phase I research effort was to demonstrate the effectiveness of plasma enhanced, high power, pulsed ion beams, produced in a Microsecond Plasma Opening Switch (MPOS) configuration, for modification of the surface properties of materials. As part of the Phase I work we constructed and tested an MPOS system which could generate up to a 300 keV ion beam and current densities up to 180 A/cm^2. The ion beam pulse duration was up to 100 ns, and the maximum energy density the system could deliver to a sample was 2.2 J/cm^2. The MPOS ion beam was used to irradiate various steel and aluminum alloy samples. Samples were rectangular 1 cm x 2 cm x 1 mm thick, 1 cm x 10 cm x 1 mm, or circular up to 2 cm in diameter and 2 mm thick. A 'grooved' aluminum sample was also irradiated to demonstrate the multidirection nature of the ion beam in the MPOS system and the capabilities of treating irregularly shaped surfaces. Steel and aluminum samples that had a pre-deposited thin film up to 500 nm in thickness of either titanium, chromium or manganese were also irradiated. Characterization of the treated samples showed structural changes to a depth of about 500 nm. Measurements indicate an increase in microhardness of a factor of about 3 can be attained for carbon steel samples, although this is likely an underestimate since the microhardness indenter makes an indentation to a depth greater than the modified surface layer. Wear and coefficient of friction measurements for steel samples do not show much improvement for the treated samples. This could be due to too high a loading during measurement of the stainless steel pin that contacts the surface and subsequent destruction of the thin modified surface layer. Corrosion resistance, as measured by mass loss, indicates a factor of at least 3 improvement can be attained for treated aluminum alloy samples. Anodic polarization curves indicate that measured corrosion currents are 3 times less for the treated aluminum samples compared to the untreated samples. Studies of microstructural changes in the surface morphology indicate a reduction in grain size for the treated samples and

the appearence of shallow craters on the surface. Crater diameter varies up to 20 microns. EDAX and Auger analysis of irradiated samples with pre-deposited thin films indicate that mixing due to ion beam irradiation occurs to a depth of up to 1 micron. In the case of a titanium film on an aluminum substrate, the microhardness of the treated surface was about that of the untreated titanium covered surface which was 50% higher than that of aluminum without the thin film coating.

Table of Contents

	Page
Cover page	
Abstract	i
Table of Contents	iii
Tables of Figures	iv
Tables	viii
Introduction	1
Main Objectives of the Phase I Program	5
Section 1: Constructing and Testing the Ion Beam Generator System	6
Section 2: Experimental Results	14
Sample Types and Configuration	14
Characterization Techniques	17
Characterization of Mechanical, Structural and Electrochemical Properties	18
Microhardness Measurements	18
Coefficient of Friction and Wear Measurements	24
Morphology Study	28
Corrosion Tests	36
Corrosion Tests on Irregular Shaped Samples and Long Strips of Aluminum	39
Samples with Pre-Deposited Thin Films	42
Future Work	53
Other Work Done by Key Personnel of Applied Pulsed Power Technologies on MPOS Modification of Material Surfaces	59
References	60

Table of Figures

Page

Figure 1: Schematic of the system. B-dot probes and a capacitive voltage divider monitor the current or voltage at the output of the main capacitor and downstream along the inner electrode. 7

Figure 2: Schematic of the trigger circuit used to trigger the main capacitor to the Plasma Opening Switch or plasma guns. 8

Figure 3: Typical V-I traces for the system when plasma is present and the device operates as an Opening Switch. 11

Figure 4: Same as figure 3 but with the 2 cm diameter cathode. 13

Figure 5: Ion beam current density as a function of position along the cathode for the two different diameter cathodes used in the Phase I work. The ion beam energy is 200 keV and the current density is measured from the first plasma gun. 13

Figure 6: Schematic of the irregular shaped aluminum samples (Upper-dimensions are in mm). Photo (lower) of the sample after it was irradiated and placed in 1% HCl for 72 hours. The darkened areas were masked and not treated by the ion beam. 15

Figure 7: Photograph of typical samples used in the Phase I work. These samples have been irradiated. The matte surface finish is the irradiated part of the sample, the other part of the sample is not irradiated because it is masked during treatment. 16

Figure 8: Microhardness as a function of depth from the surface for carbon steels c1030 (30), c1060 (60), and c1095 (95). Here the ion energy is 250 keV and the current density is 150 A/cm^2 for the c1030 sample and 120 A/cm^2 for the other samples. 20

Figure 9: Scanning electron micrographs showing cross sections of treated 1095 (upper SEM) and 1060 (lower SEM) carbon steel samples. The samples were treated using 4 pulses of an ion beam of 180 keV and current density of 100 A/cm^2. 22

Page

Figure 10: Microhardness as a function of ion beam current density for the unhardened carbon steels. 23

Figure 11: Microhardness as a function of ion beam current density for the hardened carbon steels. 23

Figure 12: Microhardness (kg/mm^2) as a function of ion beam current density for the hardened D2. The ion beam energy is about 250 keV and the current density is 150 A/cm^2. 24

Figure 13: Coefficient of friction, no lubricant. Carbon steel 1018. The beam parameters are given in the figures. 26

Figure 14: Coefficient of friction, oil lubricant. Carbon steel 1018. The beam parameters are given in the figures. 27

Figure 15: Optical micrographs showing the surface microstructure of untreated (A) and treated (B) carbon 1018 steel samples. The ion beam energy is 200 keV and the ion current density is 100 A/cm^2. 29

Figure 16: SEM of M2 steel. **A**--untreated, **B**--treated, the beam energy is 200 keV, and the current density is 100 A/cm^2. 30

Figure 17: SEM of M50 steel. **A**--untreated, **B**--treated, the beam energy is 200 keV, and the current density is 100 A/cm^2. 31

Figure 18: Optical micrograph of the surface microstructure of 1018 carbon steel. **A**--untreated, **B**--treated, the beam energy is 200 keV, and the current density is 100 A/cm^2. 32

Figure 19: Typical simulation results for irradiated iron as a function of depth into the sample. The ion beam current density is the parameter. The beam pulse length is 100 ns and the beam energy is 180 keV. The upper 'snapshot' of the temperature distribution is at the end of the 100 ns pulse and the lower graph is 100 ns after the end of the ion beam pulse. 34

Page

Figure 20: Grazing angle X-ray diffractometer results for untreated (upper) and treated (lower) 1018 carbon steel. The beam energy is 200 keV, and the current density is 100 A/cm^2. 35

Figure 21: Anodic polarization curves for 6061 (upper) and 2014 aluminum (lower) alloys. Curve **1** is for untreated samples, curve **2** is for treated samples using 5 shots and a current density of 40 A/cm^2 and curve 3 is for treated samples using 5 shots at 70 A/cm^2 current density. The ion beam energy is 180 keV. The vertical axis is measured current in microAmperes and the horizontal axis is the applied voltage in Volts. 37

Figure 22: Optical micrograph of the surface microstructure of 5083 Al alloy corroded in 1% HCl for 48 hours. **A**--untreated surface, **B**--treated surface, the beam energy is 200 keV, and the current density is 100 A/cm^2. 38

Figure 23: Optical micrographs of grooved aluminum 6061 after 48 hours in 1% HCl solution. The upper two photos show the side (upper left) and flat surface (upper right) of the untreated (masked) portion of the sample. The lower two photos show side (lower left) and flat surface (lower right) of the treated portion of the sample. 41

Figure 24: Photograph of the 10 cm long 6061 aluminum strip irradiated with a 250 keV, 100 A/cm^2 ion beam. The sample was placed in 1% HCl for 48 hours. 42

Figure 25: Profilometer scan of a thin film of chromium on a carbon steel substrate. The film thickness is about 500 nm. 43

Figure 26: SEM of irradiated chromium thin film on a 1018 carbon steel substrate. The chromium film is 500 nm thick. It appears as if surface smoothing occurs but no mixing. The ion beam energy is 250 keV and the current density is 150 A/cm^2. 45

Figure 27: SEM of 160 nm thick manganese film on a 6061 aluminum substrate. The upper SEM is the portion that is not irradiated and the lower SEM is the irradiated portion of the sample. The ion beam energy is 250 keV and the current density is 150 A/cm^2. 46

Page

Figure 28: SEM of 6061 aluminum covered with a 500 nm thick film of titanium. The upper SEM is the untreated portion of the sample and the lower SEM is the treated portion of the sample. The ion beam energy is 250 keV and the current density is 150 A/cm^2. 49

Figure 29: EDAX results at 10 kV for the untreated portion of the 6061 sample of Figure 28. At 5 kV electron beam energies the composition appears to be all titanium since the electron range in the titanium is less than 500 nm. 50

Figure 30: EDAX results at 10 kV for the treated portion of the 6061 sample of Figures 28 and 29. Additional EDAX at higher energies indicated that mixing of the titanium and aluminum likely occured. 51

Figure 31: Auger profile of a 6061 aluminum substrate covered with a thin titanium film of 500 nm thickness after irradiation with a 200 keV, 150 A/cm^2 ion beam (sample of Figures 28-30). Significant mixing of the titanium occurs to depths of 1 micron. The carbon and oxygen are likely due to the plasma constituents and surface layers. 52

TABLES

Page

Table 1: **Surface Microhardness of Aluminum and Steel Samples.** Here 'j' is the current density in A/cm^2 of the ion beam. The ion beam energy is approximately 200 keV. The D2 and M2 samples are unhardened samples having Rockwell hardness of about 28. 19

Table 2: Surface Microhardness of Carbon Steels and D2 and M2 Steels. The D2 and M2 samples are unhardened samples having a Rockwell hardness of about 28. The ion beam energy is 250 keV and the pulse duration is about 65 ns. 19

Table 3: Surface Microhardness of carbon steels and D2 and M2 steels. The D2 and M2 samples are hardened samples having a Rockwell hardness of about 62. The ion beam energy is 250 keV and the pulse duration is about 65 ns. 20

Table 4: **Weight loss of some of the aluminum samples**. A solution of 1% HCl was used for the 5083 and a solution of 5% NaCl and 0.3 H_2O_2 for the 6061 Al alloy sample. 36

Table 5: **Microhardness of titanium coated aluminum**. Microhardness measurements for the 6061 aluminum without titanium, with a 500 nm thick titanium layer and after treatment. 48

Introduction

Pulsed-power technology and High Power Pulsed Ion Beams (HPPIB) in particular have received much attention recently as a possible technology that can be used for material surface modification and production of next generation advanced materials. Several promising pulsed-power based approaches employ plasma flows and High Power Pulsed Ion Beams [1-20]. Probably the most well known of these approaches is the Los Alamos National Laboratory Plasma Source Ion Implantation device [6-8] and the HPPIB system being developed by Quantum Manufacturing Technology, Albuquerque, N.M., (see references 2-4 for a discussion of the technology of their approach) a company partially capitalized with venture capital and whose outgrowth came from work done at Sandia National Laboratory and work done in Tomsk, Russia, at the Institute of High Current Electronics and the ElectroPhysical Institute. HPPIB treatment of materials, including carbon steels, stainless steels, aluminum and polymers has resulted in improvements in corrosion and erosion resistance, microhardness, and has also resulted in microstructure changes of the materials [see references 4, 5, 7, 9, 12, 14, 15, 17-20].

The main objective of our Phase I research effort was to demonstrate the effectiveness of plasma enhanced, high power, pulsed ion beams, produced in a Microsecond Plasma Opening Switch (MPOS) configuration, for modification of the surface properties of materials. Our approach to the problem of the production of the high power ion beam pulse is unique in the field and has very important and real advantages over the competing approaches. In order to appreciate the advantages of our approach we will discuss the basic idea behind HPPIB treatment of material surfaces.

HPPIB treatment of surfaces is a thermal process that does not significantly alter the atomic composition of the sample. The implanted ion concentration, over the ion range in the sample, is typically less than 10^{-3} atomic percent. Instead, a short, usually less than 100 nanosecond, intense ion pulse is used to rapidly heat a thin surface layer to melt. The short pulse limits the effect of thermal diffusion so that rapid heating and cooling of the near surface layer occurs.

Typical cooling rates for the process can be between 10^9 to 10^{10} K/s. In principle, these cooling rates are sufficient to cause amorphous layer formation and the production of non-equilibrium microstructures including nano-crystalline and metastable phases. As previously stated, surface modification experiments using HPPIB have demonstrated that this rapid thermal quenching can significantly improve corrosion, wear and hardness properties of various materials.

We can make a simple estimate of the energy density (J/cm^2) needed to bring the sample to melting or intense evaporation (ablation). The ion beam current density required to melt or ablate the material, for a given pulse length and beam energy, can be calculated from these values given the following relation; $jV\tau = W$, where j is the current density in A/cm^2, V is the beam voltage, τ is the pulse duration and W is the energy density. The required current density for effective modification would lie somewhere between the current density needed to melt the sample surface and the current density needed to ablate the sample surface.

A straightforward estimate of the energy density required for rapid heating to melting of a sample can be made using simple physical principles. To heat a square cm of material to melting requires the following energy density, $W=C\rho\delta\Delta T$, where C is the specific heat (we assume a molar specific heat of ~ 25 J/mole-^{0}K for metals), ρ is the density of the sample, δ is a modified proton range (we assume the ion beam is mainly protons) that roughly takes into account thermal diffusion in the material during the pulse and ΔT is the difference in temperature between the initial and melting temperature. Assuming the target material is iron and a proton beam energy of 300 keV (δ ~ 2 to 3 micron) and substituting appropriate values we get W~ 1 to 1.5 J/cm^2 for the energy density needed to bring the surface to melting temperatue. This corresponds to a current density of about 50 A/cm^2 for a 100 ns pulse. An 800 keV proton energy would require a current density of about 90 A/cm^2 due mostly to the longer range of the protons and the thermal diffusion.

Intensive evaporation (ablation) occurs when the temperature reaches a critical value, for iron it is 2700 ^{o}C, for aluminum 1700 ^{o}C. The ion beam power needed for ablation can be roughly estimated from $Q^*=KT^*\delta/(\chi\tau)$ where K is the thermal conductivity, χ is the thermal diffusion rate and τ is the pulse-length. Substituting appropriate values we find that for ~ 300 keV ions the current density is ~ 140 A/cm^2 and for 800 keV ions the current density is ~ 200 A/cm^2. Therefore, we conclude that effective surface modification can occur using 800 keV protons with beam current densities between 90 to 200 A/cm^2 and for current densities between 50 to 140 A/cm^2 for 300 keV protons, again assuming a 100 ns pulse duration. Of course this is an underestimate of the actual current density required for evaporation since sublimation energies are not included (the results of a detailed calculation for temperature distribution in pure iron as a function of ion beam current density is shown in the section on morphology). The point is that the estimated values of current density, and values up to 2 times larger, are straightforward to generate using the MPOS or with vacuum ion diodes. Note that the current densities scale inversely with pulse duration, i.e. a larger current density is required for shorter pulses. Note too that the current density necessary for modification will always be greater for higher energy beams since the intrinsic ion range increases with beam energy, though the thermal wave diffusion mitigates, to some extent, this difference at longer pulse durations.

The point of the exercise is to demonstrate that relatively low energy ion beams can be used to treat material surfaces as well as higher energy beams. There is nothing 'magic' about high energy ion beams or ion beams generated in a vacuum diode. What will determine if HPPIB treatment is commercially viable will be whether the technology employed for the generation of the beams is scalable to large areas, is cost effective, is low in maintenance and user friendly.

Our MPOS system has several advantages when compared to the other approaches to thermal treatments of materials using high power ion beams. The ion beam generated in the MPOS sheath is multidirectional and can treat a sample with a complicated shape that has irregularities on a mm scale. The technology being developed by Quantum Manufacturing Technology is

based on vacuum ion beam diodes. The Quantum Manufacturing Technology approach has the limitation that the ion beam treatment is line of sight. A part with surface irregularities would have to be turned or tilted in the ion beam for total surface coverage or the ion beam would need to be swept over the part, further complicating the approach. In addition, conventional magnetically insulated vacuum ion diode systems are not efficient in converting electrical energy to ion beam energy, they are very complicated (magnetically insulated ion beam diodes require complicated magnetic fields for insulation and large energy storage to power the field coils) and very difficult to scale to large geometries. This last point is particularly important. In our studies conducted for Phase I, and in work done by other groups [e.g. 3, 5, 20], we have found that a minimum of about 50 A/cm^2 current density at about 150 keV ion energy (~ 1 J/cm^2) is needed to effectively enhance the corrosion resistance of materials like aluminum. At higher ion beam energies, like those used by Quantum Manufacturing Technology, the current density required is higher due to the longer range of the ions in the material. Scaling of the Quantum Technology approach to large surface areas, say 50 cm on a side, would require greater than several hundred kiloAmperes of ion beam current. This is a formidable task for a vacuum ion diode system. The other alternatives would be to either raster the ion beam across the part or move the part in the ion beam. This is a more costly and complex approach to the problem of materials modification.

Our MPOS system has demonstrated production of up to a total of 40 kA of ion beam current over a surface area of about 250 cm^2 in a cylindrical system geometry. This represents a conversion efficiency from stored current to switched current of about 35%. The system we currently have is easily scaled so that greater surface areas can be treated. Because of the operation of the plasma opening switch, the conversion efficiency actually increases for larger stored currents [21-23]. In addition, an MPOS system can be configured to treat surfaces that are flat, like large metal panels. In fact, previous work on MPOS systems in flat geometry has been conducted [24], although not for the purpose of material surface modification. Note too that the ion beam voltage generated by the MPOS system is much higher than the charging voltage of the system's main energy storage capacitors. This occurs because of the LdI/dt voltage increase

that results when the switch opens and the large main current is abruptly decreased. Charging voltages of a single capacitor to 45 kV can result in ion beam voltages of 250 to 300 kV using one switch. In fact higher ion beam energies can be attained by storing higher currents amplitudes in the MPOS or by increasing the charging voltage of the main storage capacitor. In contrast to this, vacuum ion beam diodes must use either pulselines and/or Marx banks to generate the high voltage. This requires more parts, the system is more complex and therefore more costly to maintain. Maintenance costs for a vacuum ion diode system capable of treating large surface areas at 300 keV energy and multi-hundred kiloAmpere currents would be very high, we estimate roughly 3 to 5 times higher than a comparable MPOS system.

Another potential advantage to the MPOS approach, although we did not attempt to exploit this or systematically explore this point, is the plasma that precedes the ion beam pulse. This plasma has a streaming energy of up to 100 eV and could provide 'degreasing' and initial preparation of the surface to be modified. Overall, we think that our approach has very real advantages that make it commercially feasible. The advantages include: relative simplicity, combination of surface preparation and treatment in a single stage, lower up-front capital costs and lower maintenance costs compared to any other HPPIB approaches; scalability (we do not believe you can go to large surface areas any other way that is practical, cost effective and user friendly), and flexibility, it is relatively straightforward to build a system that can be used for a specific geometric shape.

Main Objectives of the Phase I Program

There were two main technical objectives for this Phase I effort. The first main objective was the construction and testing of the pulsed plasma-ion beam generator (MPOS). The second main objective was the application of the pulsed ion beam generated by the MPOS to modification of various materials and to determine the effect of the ion beam treatment on characteristics like microhardness, surface roughness, wear resistance and corrosion resistance. We also treated samples that were coated with a thin layer of either chromium, titanium or manganese. The goal of this part of the Phase I effort was to demonstrate that treatment with the short pulse, high

power ion beam could cause 'mixing' of the thin film material with the substrate material. The motivation for this part of the work is based on ion beam dynamic mixing (IBDM) which occurs in conventional systems using DC ion beams of energy up to and greater than 100 keV. At these energies the irradiation leads to the formation of an intermixed layer between the film and the substrate or between two layers, and more generally to the formation of complex alloys. IBDM is an effective way to obtain very strong adhesion, and to control the structure and composition over the entire film thickness. The application of pulsed, high power, plasma-ion beams could be an effective way to engineer advanced thin film coatings with enhanced surface and adhesion properties. The following two main sections describe the results of the construction and testing of the MPOS system and the experimental results on the modification of material surfaces.

Section 1: Construction and Testing of the Ion Beam Generator System-MPOS

The construction work carried out as part of the Phase I effort involved building a vacuum system, putting together a suitable pulsed-power supply for the main capacitor and plasma gun capacitors and construction of the opening switch section (plasma-beam treatment region) as well as a data acquisition system. We modified our original system twice during the Phase I effort. The principle reason for the system changes were that the results for modification of steels like M50, M2 and D2 and the results on irradiation of samples covered with a layer of pre-deposited material, like chromium and titanium, indicated that higher energy delivery was necessary for effective modification results. However, the lower energy densities were suitable for modification of surface properties of aluminum alloys, particularly corrosion resistance enhancement. We will describe the basic system then briefly discuss the changes that were made to generate higher energy density ion beams.

A schematic of the pulsed, plasma-ion beam generator is shown in Figure 1. Not shown is the vacuum system, which is standard, and consists of a diffusion pump, roughing pump and appropriate gate valves. Typical operating pressures for the system, measured in the region of the plasma guns, is 2 to 5×10^{-5} Torr.

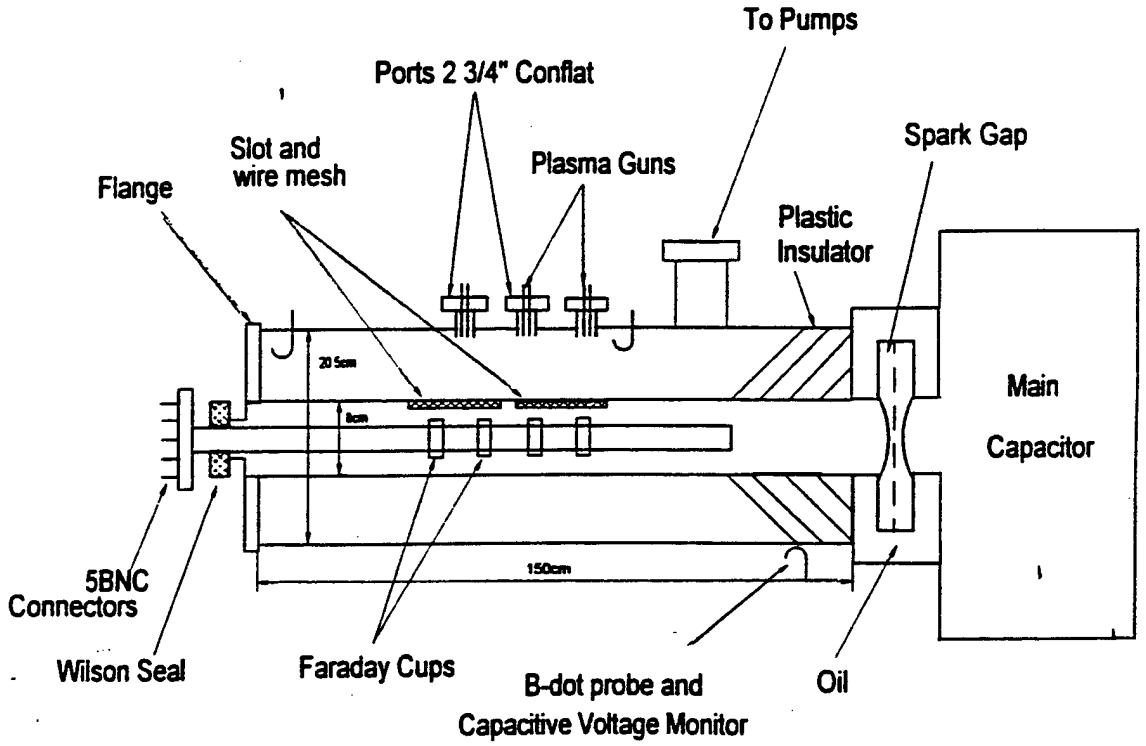

Figure 1: Schematic of the system. B-dot probes and a capacitive voltage divider monitor the current or voltage at the output of the main capacitor and downstream along the inner electrode.

The electrical system consists of charging supplies capable of charging the main capacitor and plasma gun capacitors to 50 kV, and three trigger generators as well as three delay boxes to adjust the trigger timing of the main capacitor relative to the plasma guns. The main energy storage for the system consists of a 3 μF capacitor which has a voltage rating of 100 kV and can provide a maximum of 15 kJ of stored energy. The experimental device is coaxial in geometry with the cathode of the system the inner electrode. The plasma guns are placed on the outer part

of the vacuum system and measurement of the ion beam parameters are taken from inside the hollow cathode. This system configuration is chosen because it facilitates characterization of the ion beam and plasma parameters. The main capacitor is connected to the inner electrode of the vacuum coaxial line by a triggered spark gap. The inner electrode (cathode) is grounded on the downstream side of the high voltage source by a metal end plate which is connected to the outer conductor. The outer wall of the vacuum vessel is ground and is 20.5 cm in diameter. Samples to be treated are placed on the inner conductor. The coaxial line length is approximately 1.5 meters. This includes both the inductive sections of the plasma opening switch (POS) before and after opening (the length of these sections is determined by the location of the plasma). The circuit used to switch the capacitively stored energy into the POS is shown in Figure 2. A very similar circuit is used to switch the capacitively stored energy into the plasma guns.

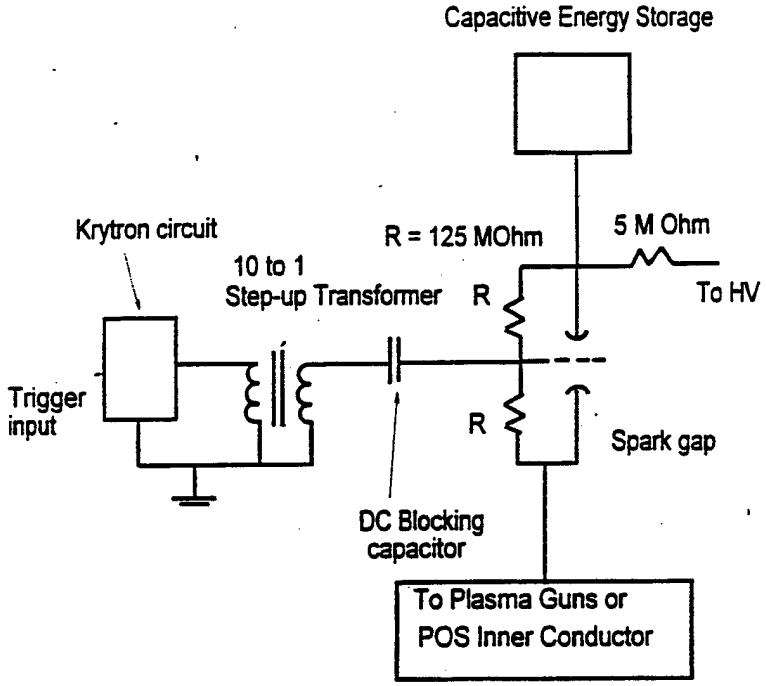

Figure 2: Schematic of the trigger circuit used to trigger the main capacitor to the Plasma Opening Switch or plasma guns.

A B-dot probe is placed at the outer periphery of the vacuum-oil insulator to monitor the net current in the system. The B-dot probe consists of a loop of wire that is oriented so that the magnetic field lines penetrate the plane of the loop. A change in magnetic field induces a current in the loop which is proportional to the current generating the magnetic field. Two downstream B-dot current probes monitor the current at locations approximately half-way from the grounded end of the system and about 15 cm from the end of the system. In addition, a capacitive voltage divider is placed at the vacuum-oil insulator to monitor system voltage. The downstream B-dot probe permits determination of any electron leakage in the coaxial line by comparing with the B-dot probe at the spark gap. Typical current flow along the inner electrode is about 120 to 140 kA.

A set of eight surface flashover plasma guns can be placed along the vacuum chamber walls. The plasma guns are placed in two groups of four with each gun spaced 90^0 apart azimuthally. We have constructed a total of 24 ports, 6 groups of 4 ports, for the 8 plasma guns so they can be positioned to give the most uniform plasma density, over the largest area possible. We can also add more guns if necessary. The set of ports are separated by 15 cm along the length of the coaxial line. The plasma guns are energized, in groups of 4, by two separate capacitors of 1.38 μF capacitance. These capacitors can also be charged to 100 kV and provide a total energy storage of 6.9 kJ. A pressurized spark gap switches the energy from these capacitors to the plasma guns. The plasma guns are connected to the output of the spark gaps by coaxial cable (RG-8). The current to the plasma guns is monitored by a small Pearson probe placed around the insulation of the inner conductor of the RG-8. The outer conductor of the cable (the return to ground for the plasma gun current) is insulated from the Pearson probe and is placed over the probe so that net current through the Pearson probe is measured. We can monitor the current through each of the 8 plasma guns separately on each shot. Monitoring the current through the guns permits determination of the time delay between the plasma gun pulse and the main capacitor discharge. We used only the 4 plasma guns closest to the vacuum-oil insulator throughout these experiments.

The inner conductor has slots covered with stainless steel screens that are cut lengthwise along the conductor. The slots are positioned azimuthally around the inner conductor. We have four biased Faraday cups placed inside the inner conductor, under the stainless steel screens, to monitor the ion beam current that passes through the screens. The cups consist of a graphite collector in a shielded housing. Two magnets for each cup provide a sufficient field to prevent electrons from being collected on the graphite collector. Bias on the cups can be up to 100 Volts. The axial position of the Faraday cups can be varied so that the ion beam current as a function of position along the inner conductor can be measured.

The operation of the system is as follows: The main energy storage capacitor and plasma gun capacitor are each charged, typically up to a maximum of 45 kV and 30 kV, respectively. After charging, a trigger signal triggers the spark gap which fires the plasma guns. After a delay of about one microsecond the main spark gap is triggered and the main storage capacitor generates current in the plasma. This is accompanied by current penetration in the plasma and translation of the plasma along the axis. After the formation of the sheath near the cathode, generation of the high energy ion beam occurs when the plasma 'opens', i.e. the plasma is no longer able to carry the current flow. The rapid change in the current due to the 'opening' generates a high voltage spike due to the inductance of the system (LdI/dt) . The high voltage generates an ion beam in the plasma which irradiates the sample surface providing the energy needed for the modification. Figure 3 shows a typical voltage and current trace for the system when plasma is present. The 'kink' in the voltage and current traces are due to the opening of the plasma. This occurs when the plasma cannot conduct the current provided by the main capacitor. The large, narrow signal which occurs at approximately 3.25 μs is the inductive voltage spike, which is about 3 times greater than the charging voltage (the first and much longer peak) for this configuration of the system which uses an 8 cm inner conductor. The peak voltage corresponds to about 140 kV. We have also shown a Faraday cup signal which indicates the presence of the ion beam during the inductive voltage spike and the plasma gun signal which shows relative timing. The specific energy delivered in this shot is estimated to be ~ 1.5 J/cm^2.

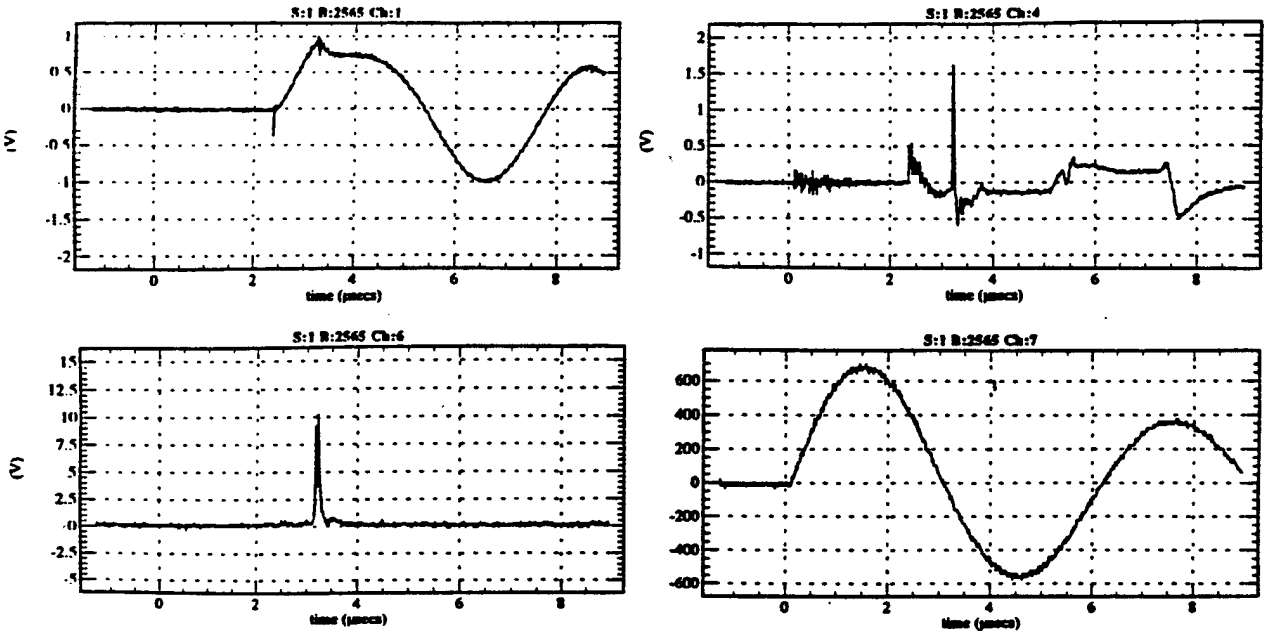

Figure 3: Typical V-I traces for the system when plasma is present and the device operates as an Opening Switch. The top left hand trace is the system current monitored at the output of the main capacitor (vacuum-oil interface), the top right hand trace is the voltage monitor. The lower left hand trace is the ion beam signal and occurs during the voltage spike which is about 3 times higher than the charging voltage and corresponds to about 140 kV. The lower right hand trace is the current in the plasma guns.

As mentioned above, we modified the system several times to provide both higher energy and higher current density ion beams. The system changes consisted principally of replacing the

inner conductor with a smaller diameter conductor (~ 2.5 cm diameter instead of the original 8 cm diameter) and rebuilding the Faraday cups necessary to map out the ion beam current density for the new geometry. We also modified the main switch geometry so that we could charge the main storage capacitor to 45 kV without problems of self-breakdown. This included outfitting the system with sulfurhexaflouride gas for the main switch. These modifications resulted in the system being capable of generating ion beam energies of up to 250 keV and current densities of up to 180 A/cm^2 for pulse durations of about 100 ns. This corresponds to an energy density delivery, taking the pulse shape into account, of up to 2.2 J/cm^2. Figure 4 shows a typical set of traces for the smaller diameter inner conductor. Note the larger high voltage spike that is generated compared to that generated when the larger inner conductor is used. In this case the ion beam energy is about 5 times greater than the charging voltage.

We stress that the system ratio of inner to outer conductor geometry and volume is what determines the magnetic field at the inner conductor in the system and hence the generation of the high voltage spike. We did not increase the outer conductor because it was not practical to do so since it would have required a complete reconstruction of the system. It was much easier to change the inner conductor and modify the connectors to the main spark gap switch. Figure 5 gives the measurement of ion beam current versus axial position measured from the first plasma gun for both inner conductors. Note that only the first four plasma guns are energized.

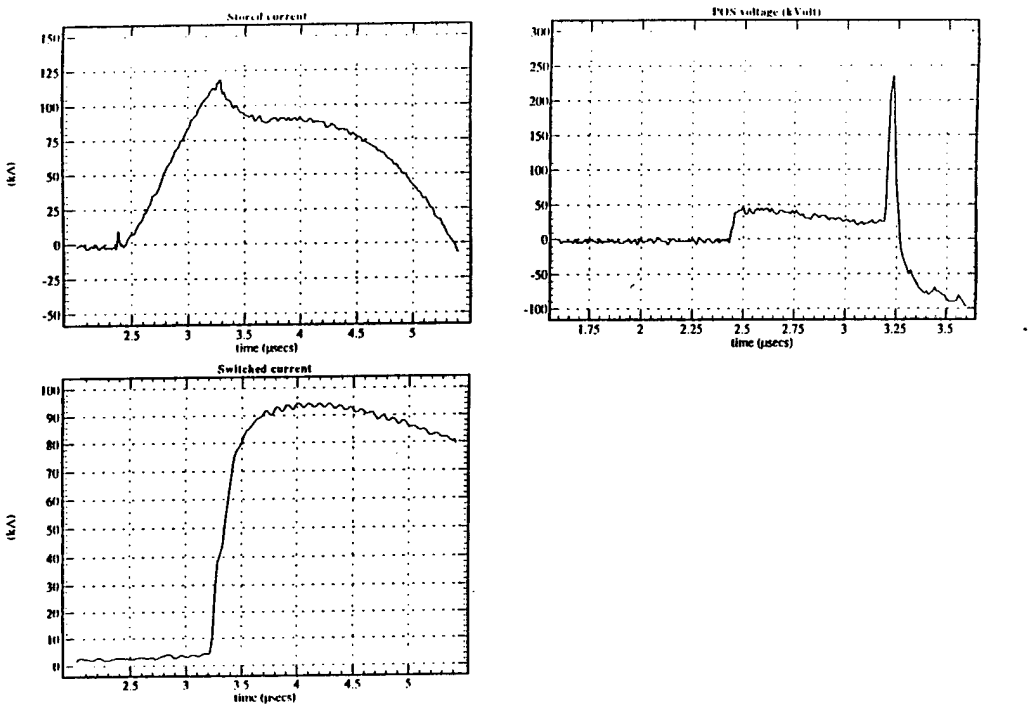

Figure 4: Same as figure 3 but with the 2 cm diameter cathode. Here the 'spike' is about 5 times larger than the charging voltage which is 45 kV.

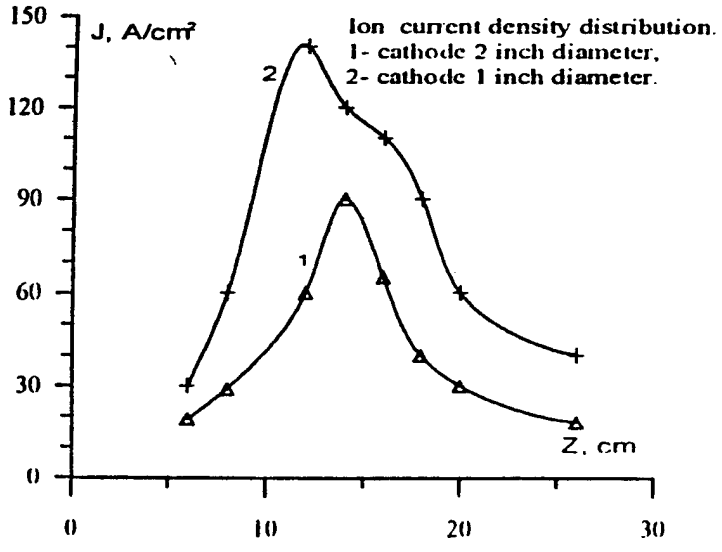

Figure 5: Ion beam current density as a function of position along the cathode for the two different diameter cathodes used in the Phase I work. The ion beam energy is 200 keV and the current density is measured from the position of the first plasma gun.

Section 2: Experimental Results

Sample Types and Configuration

The main goal of this part of the Phase I effort was to treat various metal samples with the ion beam generated by the MPOS. In addition, we also irradiated carbon steel and aluminum samples that had a pre-deposited thin film of either chromium, titanium or manganese. The goal here was to determine if mixing would occur as a result of the ion beam irradiation.

The aluminum and carbon steel samples that were treated were 1 cm x 2 cm by 1 to 2 mm thick. To estimate the total surface area our system could treat we also irradiated aluminum 'strips' 1cm x 10 cm x 1mm. The aluminum alloys that were treated included 6061, 2024, 2014, 5083 and 7075. We also treated 6061 and 2024 aluminum samples that were irregular in shape. The irregularity consisted of 2 mm grooves machined into the surface of the aluminum samples. The thickness of these samples was 5 mm. Figure 6 shows a schematic and photograph of the irregular shaped samples we treated.

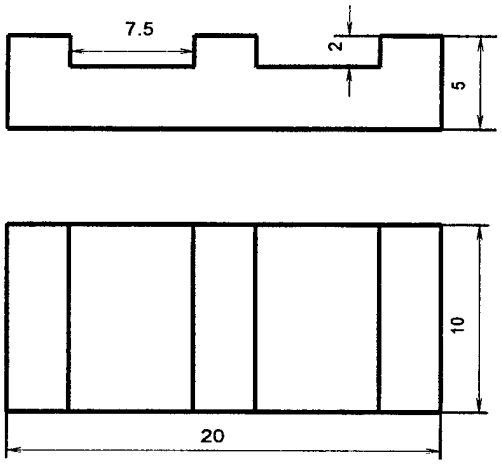

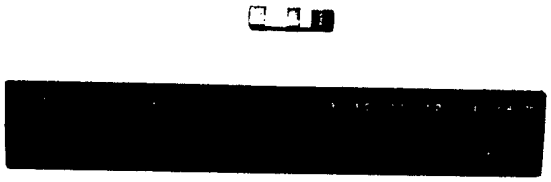

Figure 6: Schematic of the irregular shaped aluminum samples (Upper-dimensions are in mm). Photo (lower) of the sample after it was irradiated and placed in 1% HCl for 72 hours. The darkened areas were masked and not treated by the ion beam.

The carbon steel samples were of varying carbon composition and included 1018, 1030, 1060 and 1095. We treated samples that were unhardened by conventional heat treatments and we also treated samples after hardening by conventional heat treatments. Heat treating was done by a local company, MilSpec, of Huntington Beach. We also treated samples of M50, M2, and D2. These samples were round in shape and varied in diameter from 1 to 2 cm. The sample thickness was also between 1 to 2 mm. Figure 7 shows a photograph of typical rectangular and round samples. As part of the work performed during Phase I we also coated samples of carbon steel and aluminum with layers of either titanium, manganese or chromium. Layers varied in thickness from 160 nm to 500 nm. The coated samples were all 1 cm x 2 cm x 1mm thickness. After cutting the samples from stock, the samples were polished using conventional metalographic techniques. Additional polishing using alumina then diamond compound was also used on the samples that were going to be covered with the coatings. The samples were also degreased before the coatings were applied.

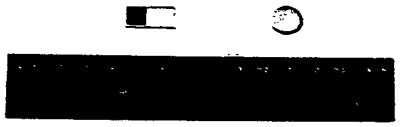

Figure 7: Photograph of typical samples used in the Phase I work. These samples have been irradiated. The matte surface finish is the irradiated part of the sample, the other part of the sample is not irradiated because it is masked during treatment.

We could mount up to 8 samples for treatment around the 8 cm diameter cathode but when we used the smaller diameter cathode, only 3 samples could be mounted for treatment. We mounted the samples onto the cathodes using copper tape of 100 micron thickness. The section of the sample that was covered by the copper tape remained untreated since the ion beam range was never sufficient to penetrate this thickness of material. Therefore, we had treated and untreated areas on the same sample so that comparison studies of the surface properties could be made. Once the samples were mounted, the cathode was inserted into the system and then the system was pumped to operating pressures of between 2 to 5 x 10^{-5} Torr. Typically, between 1 to 5 shots were used to effect the surface treatment.

Characterization Techniques

Characterization of the surface properties was carried out using standard techniques. Microhardness was measured on the surface and cross-sections of the samples using a Buehler Micromet 2004 Microhardness Tester. All results for the microhardness measurements that follow are given in Vickers hardness using a load of 10 grams. Wear and coefficient of friction measurements were done by ARL personnel on site at Aberdeen Proving Grounds.

Microstructure of the as-treated surfaces and the transverse cross-sections of the samples was observed with an optical microscope, an Axioplan with Zeiss optics, and a Philips EL30 Field Emission Scanning Electron Microscope with EDAX attachment. We also characterized the surface using a Siemens D5000 Diffraktometer and thin film attachment. Composition of the samples with the thin films was determined using the EDAX attachment to the Philips Field Emission Microscope. We also had Auger spectroscopy done at a local company called Photometrics, Incorporated, located at 15151 Springdale St., Huntington Beach, CA.

The corrosion tests were done in a variety of ways. Simple tests were carried out by placing treated and untreated samples in 1% HCl solutions or 5% NaCl and 0.3% H_2O_2 solutions and

then measuring the relative mass loss. Anodic polarization curves were also measured for the treated and untreated samples.

Characterization of Mechanical, Structural and Electrochemical Properties

Microhardness measurements

Tables 1, 2 and 3 give the results for microhardness measurements on aluminum and different steels using a load of 10 g. As can be seen in Table 1 there is no discernible increase in the microhardness for the aluminum samples. This is typical for aluminum samples and has been observed in other work on irradiation of aluminum alloys with high power ion beams. The Al 6061 alloy includes about 1.2% of Mg. The solubility curve of Al-Mg system shows that with heating the Mg is not dissolved in the Al and the system hardness does not increase, i.e. Al 6061 microhardness and plasticity cannot be changed with thermal treatment. This agrees with our results. The slight decrease of the microhardness value could be related to the ion beam thermal relief of microstresses (generated by the polishing) just below the surface.

We measured the microhardness for carbon samples, and M2 and D2 samples that were not pre-hardened by heat treatment (Tables 1 and 2) and for samples that were pre-hardened by conventional heat treatment (Table 3). The microhardness actually decreases for the stainless steel sample, SS304 (Table 1) and at modest beam current densities for the 1095 and D2 pre-hardened samples of Table 3. The reduction in microhardness using 'modest' ion beam current densities on stainless steel has been seen in previous work [17]. Note however, that the microhardness increases for the pre-hardened 1095 and D2 if the beam current density is increased past a threshold and that the microhardness always increases for the unhardened samples.

Microhardness was measured at the samples surface and along the cross-sections at different depths from the ion-treated surface for the carbon steels 1030, 1060 and 1095 and is shown in

Figure 8 below.

j A/cm^2	2014 Al	6061 Al	5083 Al	SS 304	C 1018	C1018	D2	M2
j_i=0	173	120	112	445	265	172	295	300
j_i<40	169	119	-	426	-	-	-	-
j_i=60	166	123	-	342	341	-	380	400
j_i=80	175	128	114	321	343	286	478	-
j_i=100	172	132	122	320	360	269	-	550

Table 1: Surface Microhardness of Aluminum and Steel Samples. Here 'j' is the current density in A/cm2 of the ion beam. The ion beam energy is approximately 200 keV. The D2 and M2 samples are unhardened samples having Rockwell hardness of about 28.

sample	c1030	c1060	c1095	D2	M2
untreated	208-212	224	208-230	235	274
j = 80 A/cm^2			366	366	372
j = 100 A/cm^2	320				
j = 120 A/cm^2		595	527		
j = 150 A/cm^2	443				

Table 2: Surface Microhardness of Carbon Steels and D2 and M2 Steels. The D2 and M2 samples are unhardened samples having a Rockwell hardness of about 28. The ion beam energy is 250 keV and the pulse duration is about 65 ns.

sample	c1030	c1060	c1095	D2	M2
untreated	388	426	489	645	571
j = 80 A/cm^2	449	614		581	
j = 100 A/cm^2		733			
j = 110 A/cm^2			744		
j = 120 A/cm^2	555				634
j = 140 A/cm^2				826	

Table 3: Surface Microhardness of carbon steels and D2 and M2 steels. The D2 and M2 samples are hardened samples having a Rockwell hardness of about 62. The ion beam energy is 250 keV and the pulse duration is about 65 ns.

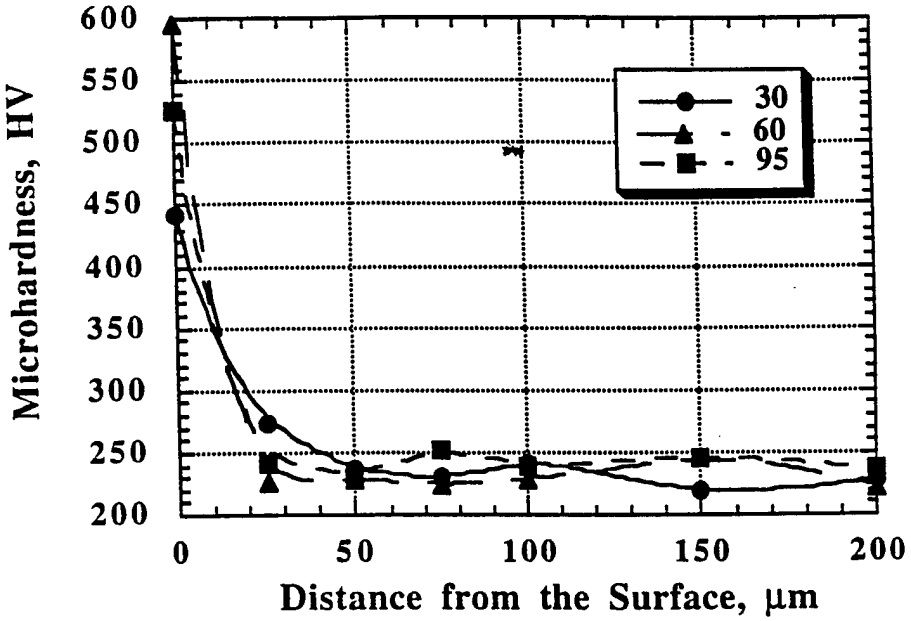

Figure 8: Microhardness as a function of depth from the surface for carbon steels c1030 (30), c1060 (60), and c1095 (95). Here the ion energy is 250 keV and the current density is 150 A/cm^2 for the c1030 sample and 120 A/cm^2 for the other samples.

The microhardness versus depth measurements, done on the cross-sectioned samples, need to be considered keeping in mind that it is extremely difficult to place the load bearing tip with accuracy greater than about 10 microns. In addition, based on the results of the SEM studies on cross-sections of treated samples (see Figure 9, below), it is clear that appreciable change in microhardness is not likely to occur for depths greater than about 1 micron.

Figures 10 through 12 show the results of microhardness as a function of ion beam current density for most of the data we have accumulated to date. We feel the measurements are more than likely an underestimate of the microhardness. The reason being that the thickness of the affected surface layer, at the specific energies delivered, is less than the indentation depth of the load bearing tip, which is at least several microns. In any event, it is clear that the microhardness increases for the non-stainless steel samples, with increasing current density, whether they are initially hardened or not.

Our conclusions are that change in surface hardness is best measured using nano-indentation. This is due to the fact that, for the energy densities delivered to the samples, the affected surface layer is about 500 nm thick. Given the typical tip sizes used to measure microhardness, the indentation is clearly deeper than the affected surface layer, even when a load of 10 grams is used. However, increases in the microhardness of the treated surfaces are clearly evident and the scaling trend is that the microhardness increases with increasing energy density delivered to the surface.

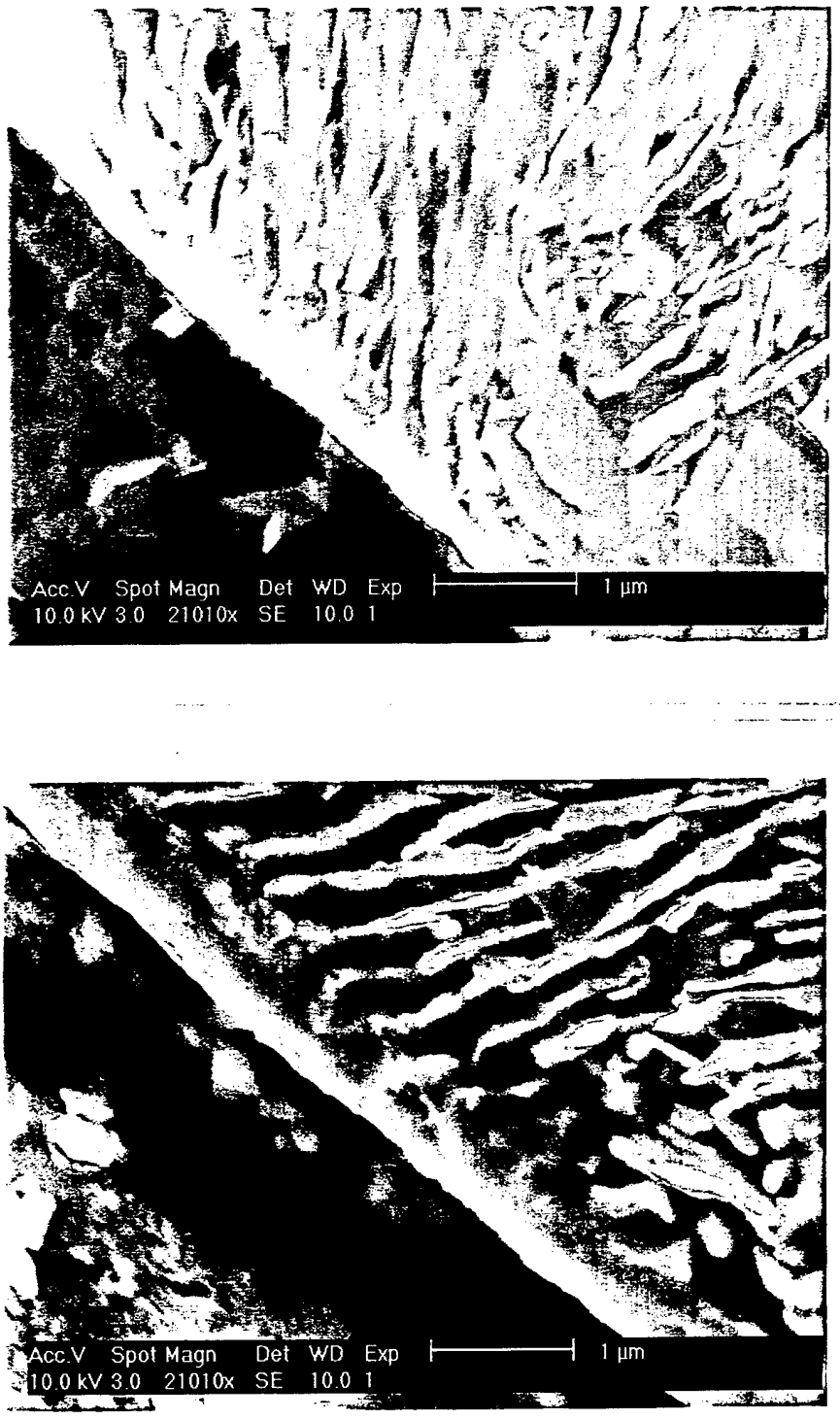

Figure 9: Scanning electron micrographs showing cross sections of treated 1095 (upper SEM) and 1060 (lower SEM) carbon steel samples. The samples were treated using 4 pulses of an ion beam of 180 keV and current density of 100 A/cm^2.

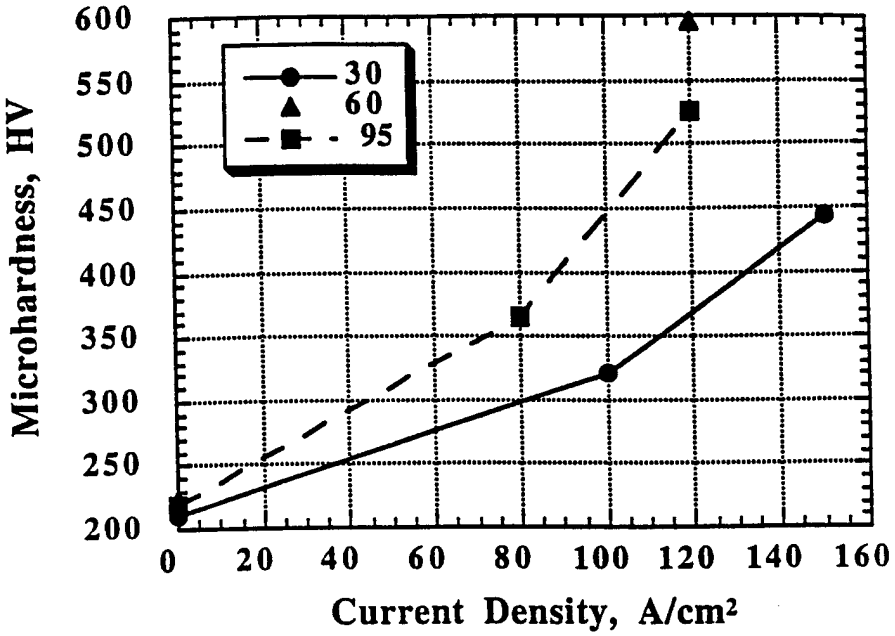

Figure 10: Microhardness as a function of ion beam current density for the unhardened carbon steels.

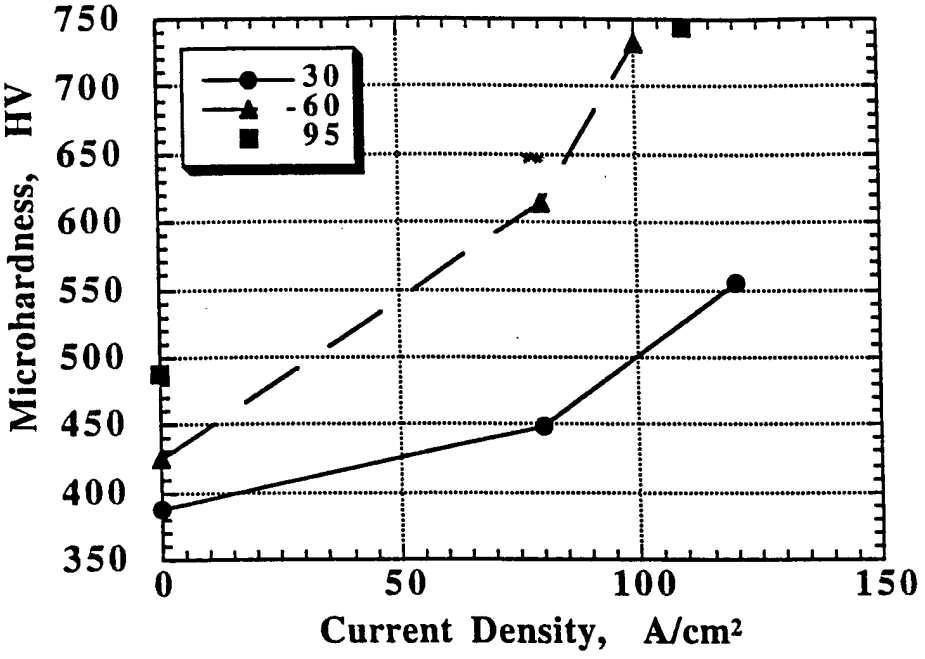

Figure 11: Microhardness as a function of ion beam current density for the hardened carbon steels.

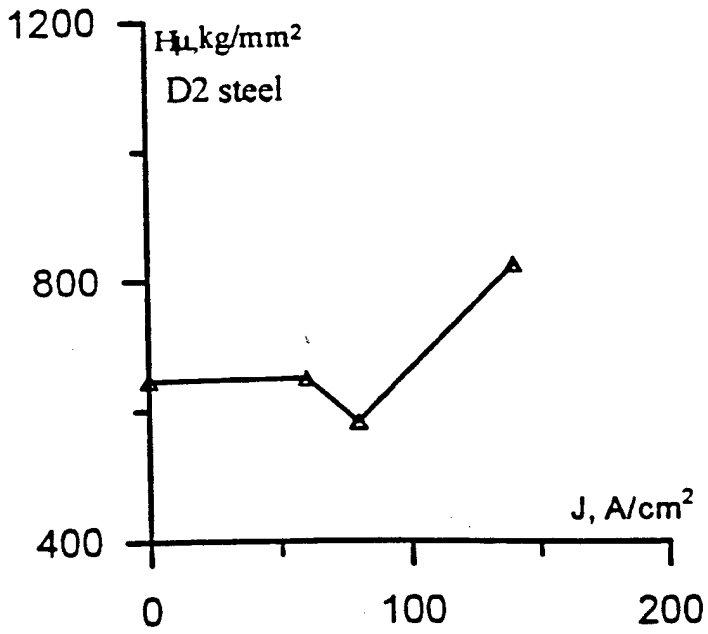

Figure 12: Microhardness (kg/mm^2) as a function of ion beam current density for the hardened D2. The ion beam energy is about 250 keV and the current density is 150 A/cm^2.

Coefficient of Friction and Wear Measurements

We sent a set of treated and untreated samples to the Metals Research Branch of the Army Research Laboratory for determination of the change, if any, in the coefficient of friction and wear characteristics. The set of samples were 1018 carbon steel. The coefficient of friction was measured using a 440 stainless steel pin at a loading of 100 grams by Dr. Constantine Fountzoulas. These measurements were done before the cross sectioning and SEM work which indicates that the surface layer changes occur to a depth of about 500 nm. It seems that a more appropriate loading on the steel pin that makes the wear track in the sample should be much less than 100 grams.

The coefficient of friction was measured dry and with oil as a lubricant. The results for the dry testing indicate that the untreated sample, generally speaking, showed a lower coefficient for a longer distance of travel of the pin. It is not clear why this is the case except that, as noted below, the surface of the treated steel samples, for ion beam current densities greater than about 50 A/cm^2, generally showed 'craters' of up to 20 micron diameter dispersed on the surface of the sample. This was not the case for the M50 (see Figure 17) but we have not had the M50 tested yet. Figure 13 shows typical results for the coefficient of friction measurements without lubricant.

The results for the measurement when oil is used as the lubricant can be seen in Figure 14 above. The best results seem to be for the case when the sample is irradiated with the lower current densities. This may be due to the lack of craters on the surface. It is interesting to note that a similar result, i.e., lower current densities resulted in decreased coefficient of friction and lower rate of wear, was found with stainless steel samples in other work [17]. We did not know of the results of reference 17 until recently and so we did not have the opportunity to treat samples at relatively low current densities and have them tested by ARL personnel.

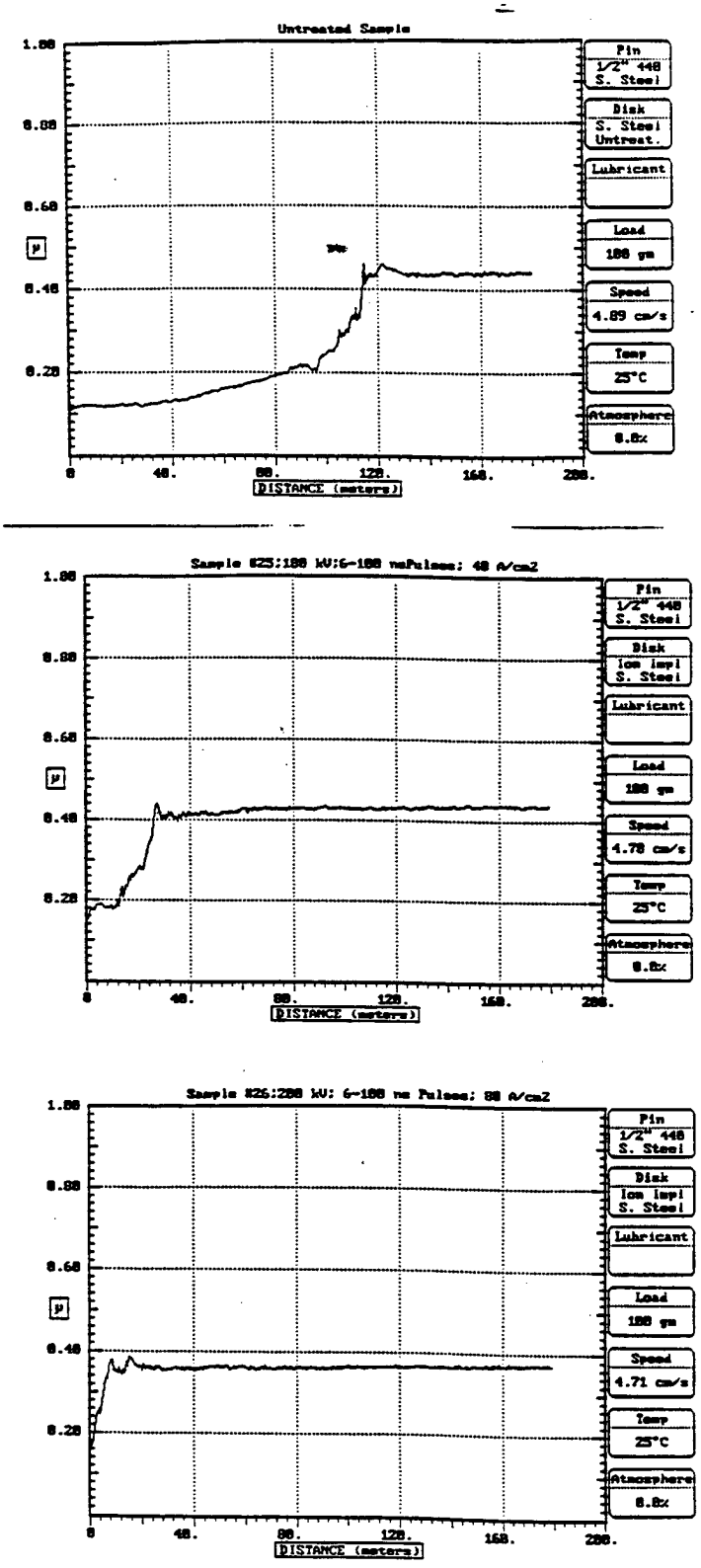

Figure 13: Coefficient of friction, no lubricant. Carbon steel 1018. The beam parameters are given in the figures.

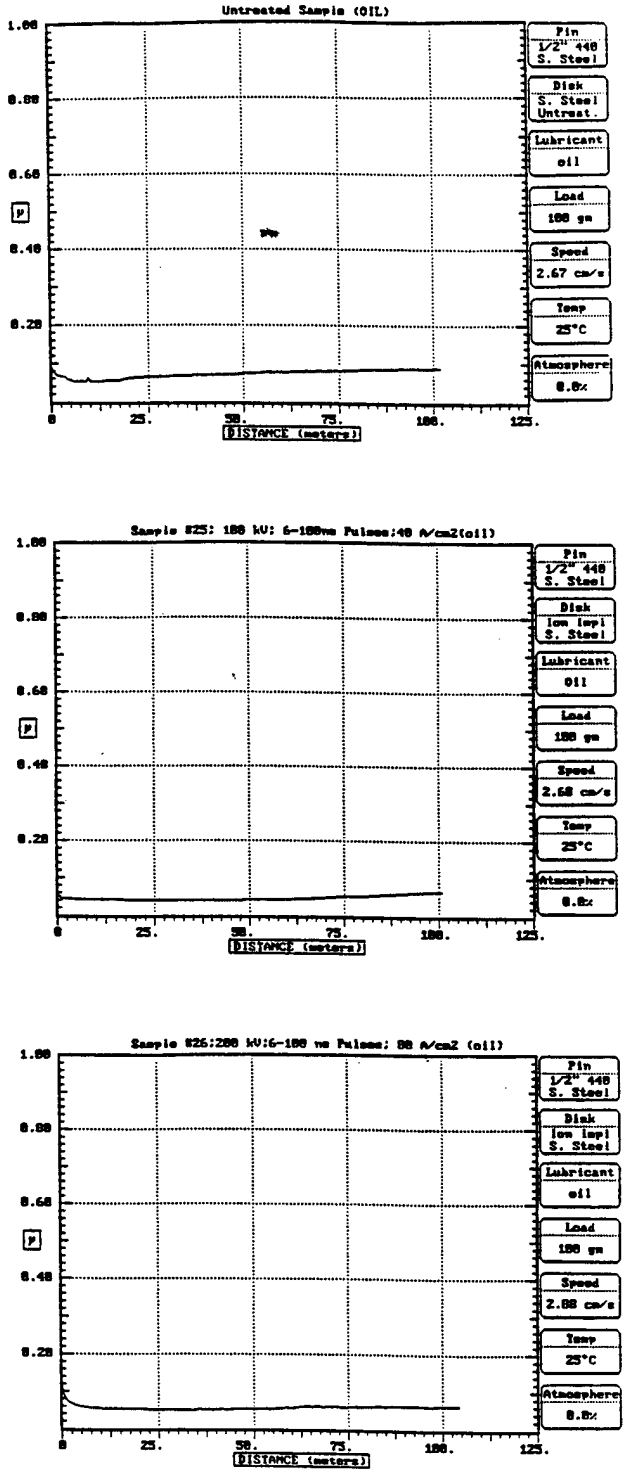

Figure 14: Coefficient of friction, oil lubricant. Carbon steel 1018. The beam parameters are given in the figure.

Morphology Study

Typical micrographs of the ion treated samples are presented in Figures 15 to 18. The energy of the ion beam was in the range of 150 to 200 keV. Craters were produced (see Figure 15 for example) at the samples surface for the carbon steels using an ion current density of $j_i > 50$ A/cm^2 and for aluminum at ion current densities greater than 30 A/cm^2. Most of the craters on the treated surfaces are several microns in depth and have a diameter of about 10 to 20 μm and are distributed over the whole region of the treated surface. These craters appear to exhibit a circular geometry. Based on the data for the ion current density and energy we estimate the specific energy input thresholds for surface melting in the case of Al alloy and steel samples are 1.0 and 1.6 J/cm^2, respectively. This agrees well enough with our estimates given in the introduction. Craters were not observed in the carbon steel samples with a current density of 50 A/cm^2 or lower. In addition, craters were not observed in the treated M50 even at 100 A/cm^2 current density (see Figure 17).

Melting of the surface is accompanied by pronounced changes in the surface microstructure and surface smoothing. It is clear from Figure 18 that the microstructure of the ion treated region is much different from that of the untreated region. A refined microstructure was obtained in the treated surface of the carbon steel sample, likely due to the rapid solidification of the surface melt. Significant change in the surface morphology was also observed on the treated surfaces of the stainless steel samples and the Al alloys.

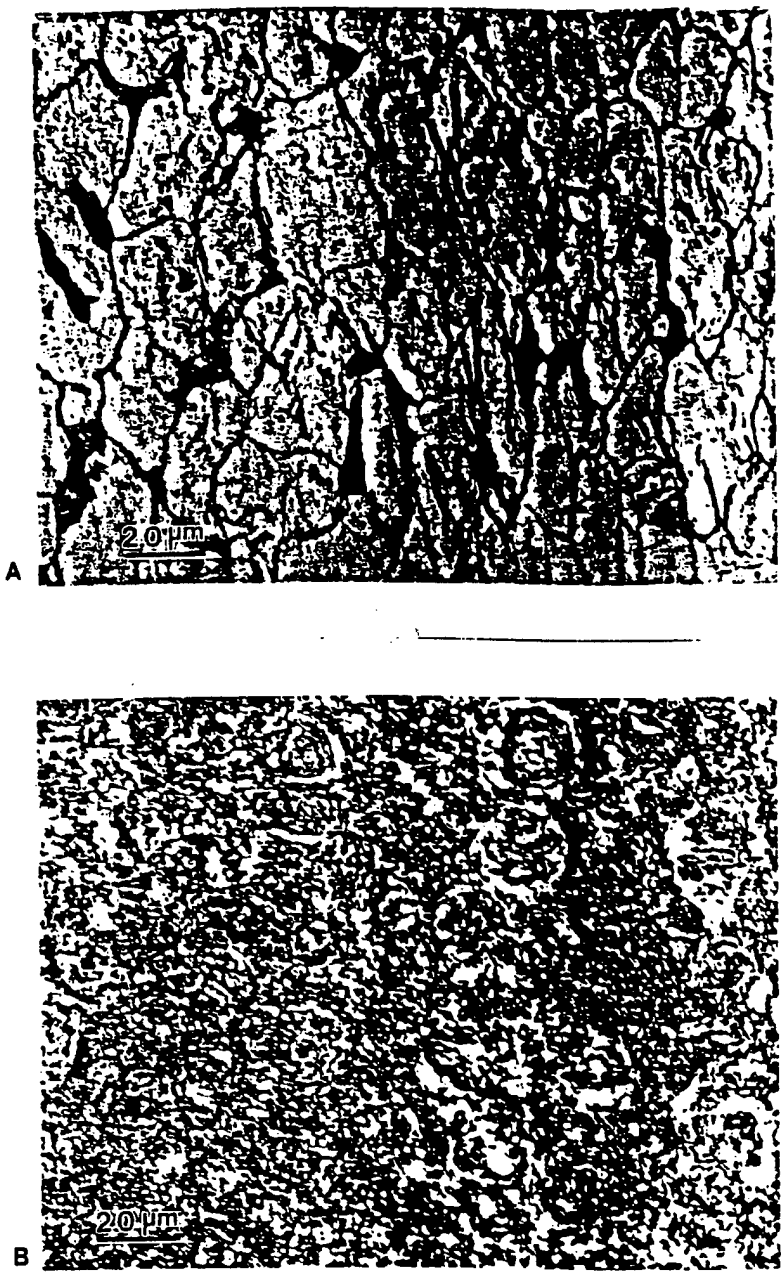

Figure 15: Optical micrographs showing the surface microstructure of untreated (A) and treated (B) carbon 1018 steel samples. The ion beam energy is 200 keV and the ion current density is 100 A/cm^2.

A.

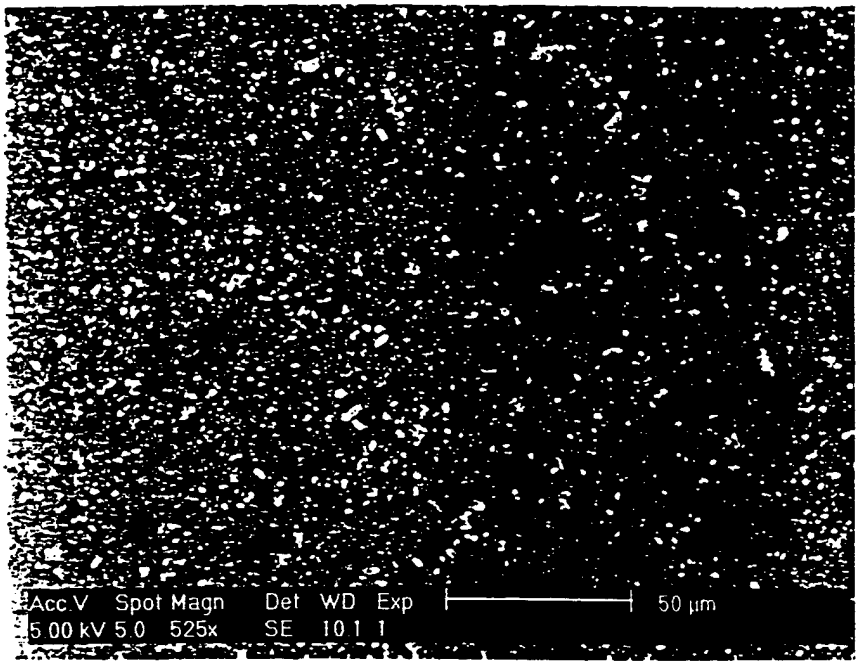

B.

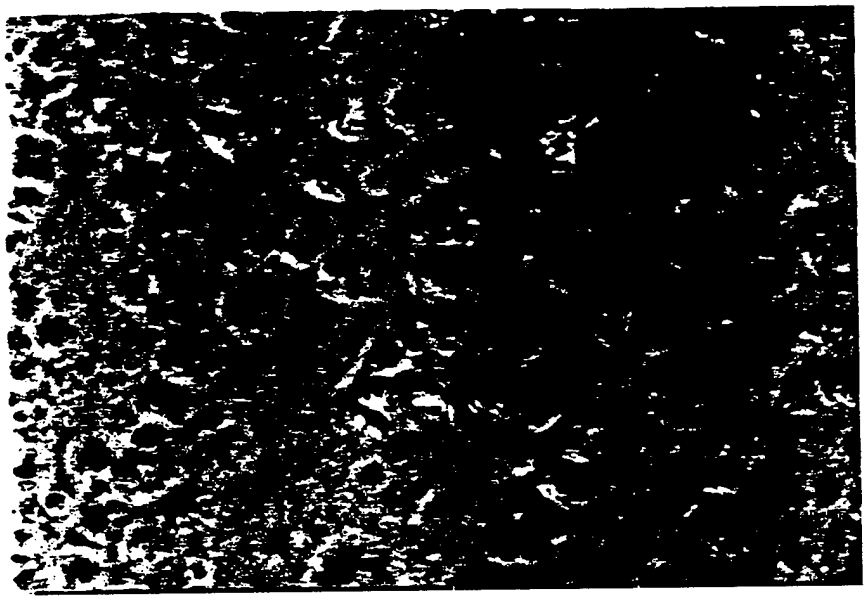

Figure 16: SEM of M2 steel. **A**--untreated, **B**--treated, the beam energy is 200 keV, and the current density is 100 A/cm^2.

A

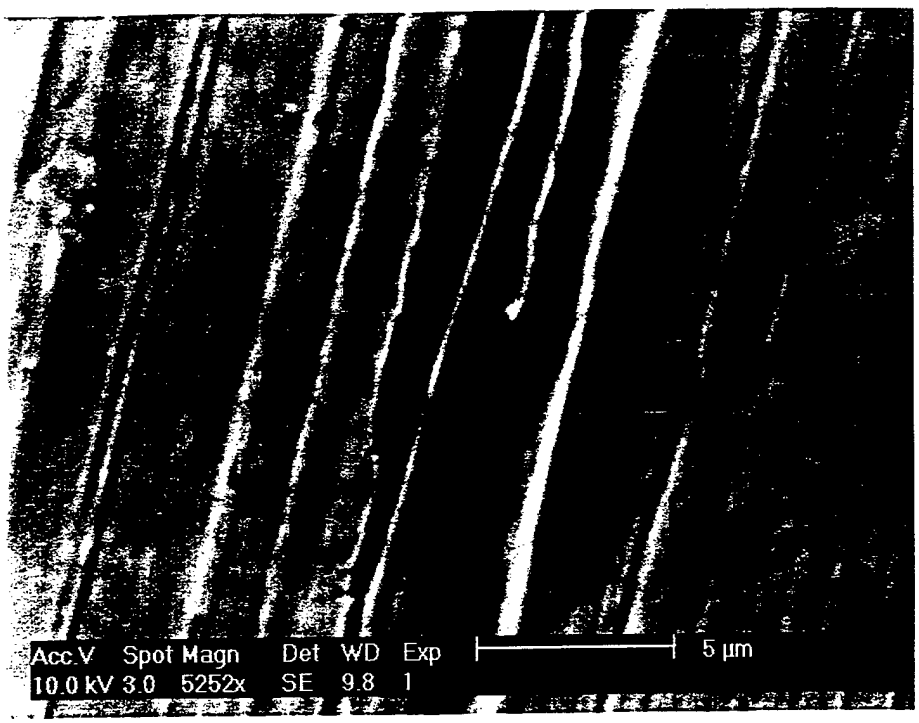

B

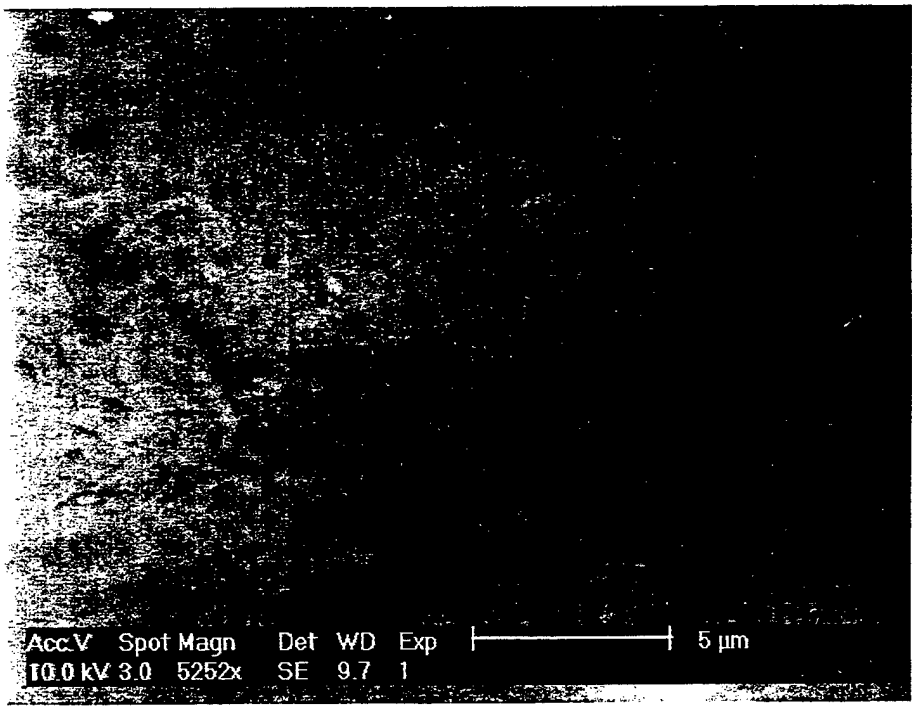

Figure 17: SEM of M50 steel. **A**--untreated, **B**--treated, the beam energy is 200 keV, and the current density is 100 A/cm^2.

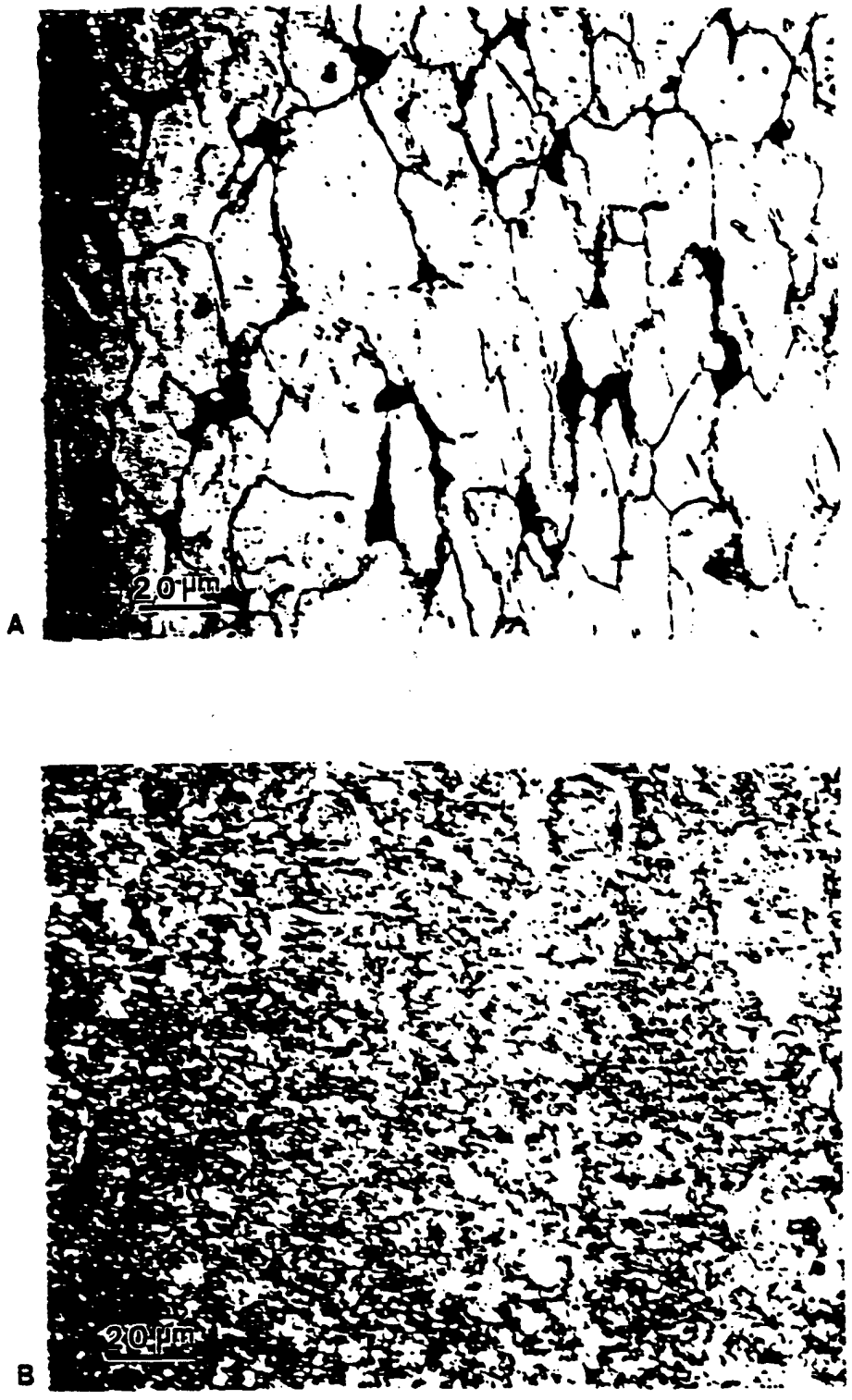

Figure 18: Optical micrograph of the surface microstructure of 1018 carbon steel. **A**--untreated, **B**--treated, the beam energy is 200 keV, and the current density is 100 A/cm^2.

Computer simulations of surface layer temperature dynamics for ion beam interaction with Al and Fe samples, for parameters similar to our experimental conditions, (ion beam energy of 180 keV, ion beam composition of H^+ and C^+, and current density between 60 to 150 A/cm^2) are in good agreement with the experimental results. A typical numerical calculation for iron is shown in Figure 19 with the ion current density a parameter. These calculations were done for us by a group at the Tomsk Electro-Physical Institute, Tomsk, Russia. According to simulations, a current density of about 100 A/cm^2 is the threshold for surface melting. Figure 19 also shows the temperature distribution 100 ns after the end of the ion beam pulse. The average cooling rate of a 1 micron thick surface layer, deduced from these simulations, is about $5x10^9$ K/s for steel.

Based on the numerical calculations, we have done grazing angle incidence diffractometer studies on treated and untreated samples both with and without thin film layers. The angle of incidence was 2^0 and the X-ray energy was 8 kV. Some of the results indicate a decrease in grain boundary structure for the treated samples compared to the untreated ones. This is inferred from the fact that the width of the peaks in the diffractometer scans is increased for the treated samples. We have estimated that the range of the X-rays for the 2^0 angle of incidence is greater than one micron. Therefore, the broadening we see in the case of the treated samples is less than what might be expected since the X-rays sample some of the underlying structure of the material (the affected region is about 500 nm thick). Generally, the diffractometer results are in agreement with the optical and scanning electron micrographs we have taken of the samples. We have not been able to quantify the difference in grain sizes at this time. Figure 20 shows a typical result for a carbon steel 1060 sample before treatment and after ion beam treatment, respectively.

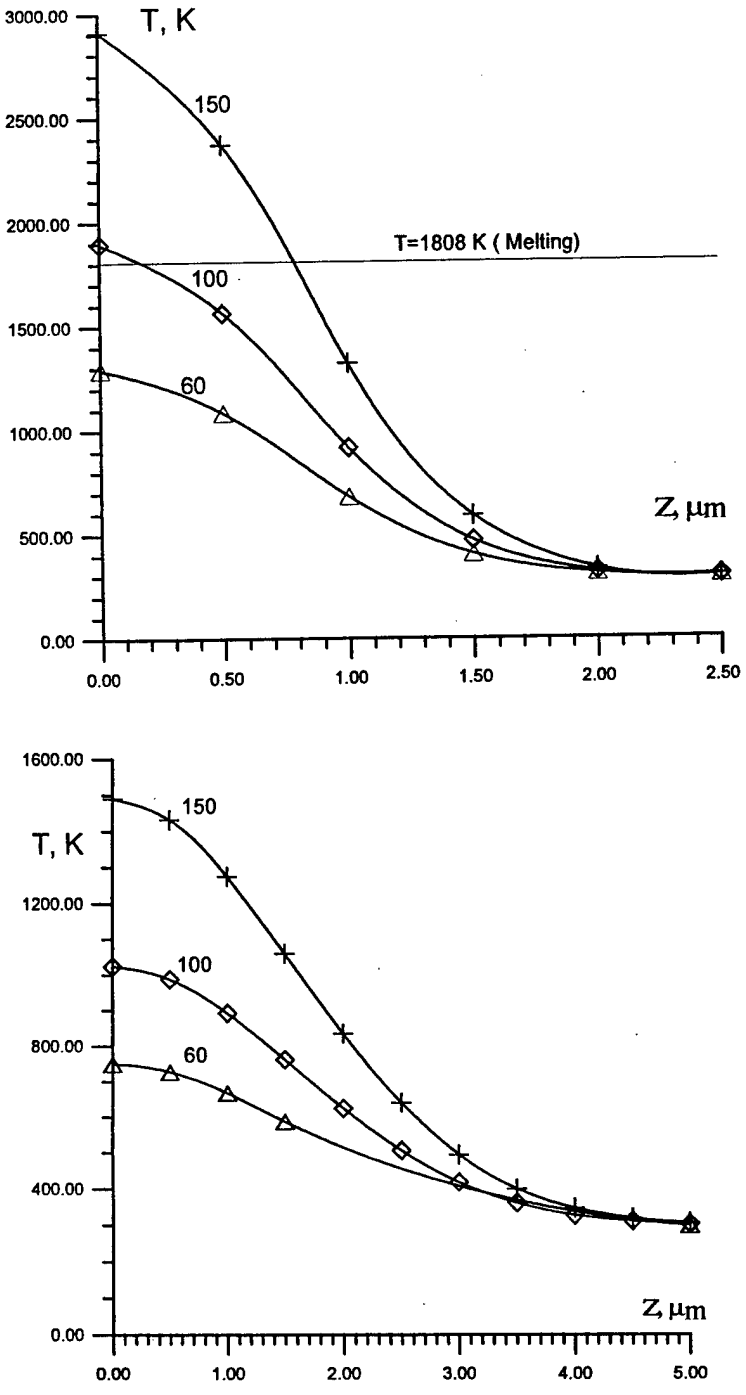

Figure 19: Typical simulation results for irradiated iron as a function of depth into the sample. The ion beam current density is the parameter. The beam pulse length is 100 ns and the beam energy is 180 keV. The upper 'snapshot' of the temperature distribution is at the end of the 100 ns pulse and the lower graph is 100 ns after the end of the ion beam pulse.

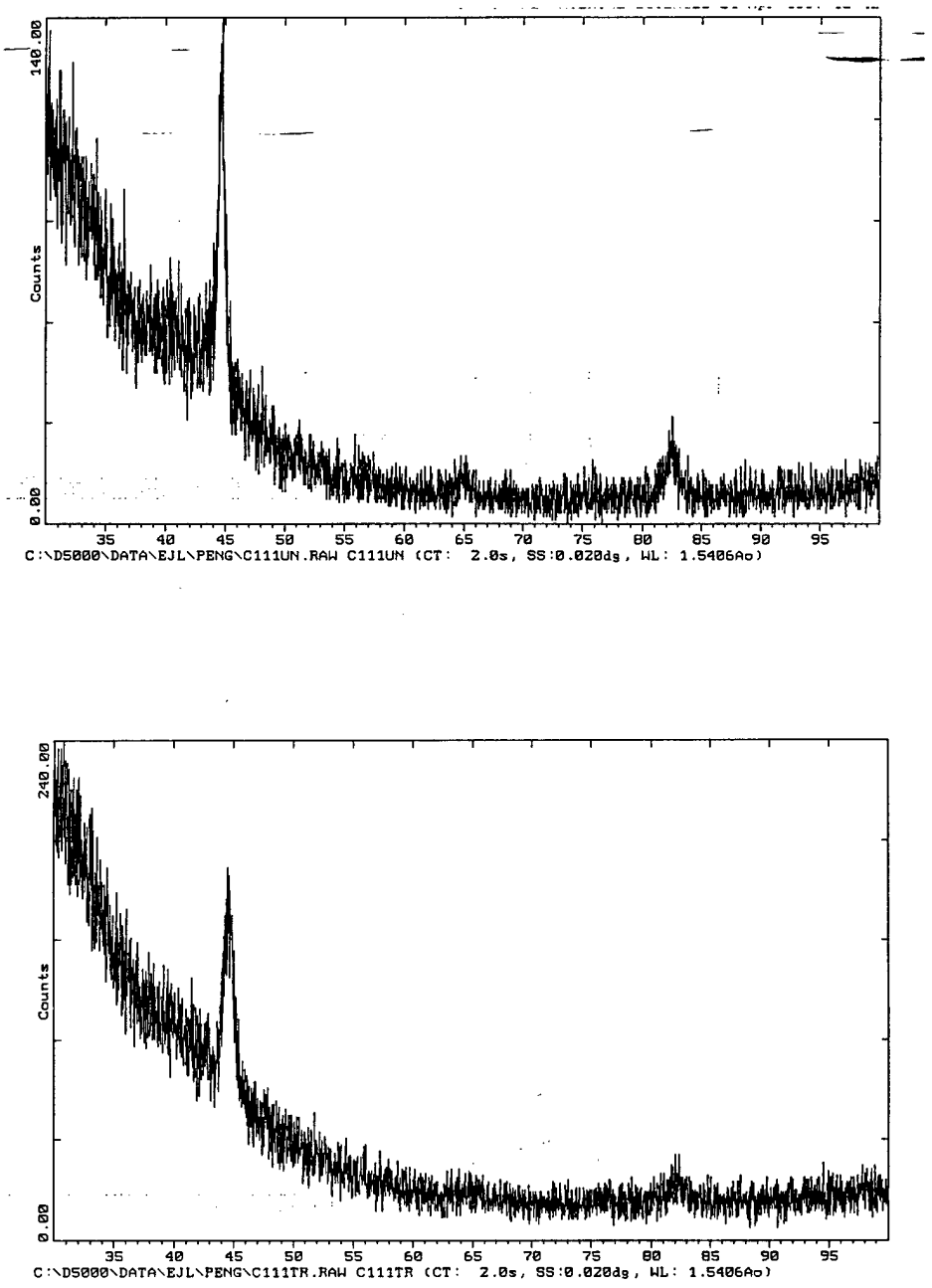

Figure 20: Grazing angle X-ray diffractometer results for untreated (upper) and treated (lower) 1018 carbon steel. The beam energy is 200 keV, and the current density is 100 A/cm^2. Some broadening of the peak occurs indicting a change in grain size due to ion beam irradiation.

Corrosion Tests

A weight loss method was used for the corrosion tests on the 2014, 6061 and 5083 Al alloy samples. A solution of 1% HCl was used for 5083 and 2014 Al alloy samples and a solution of 5% NaCl and 0.3 H_2O_2 for the 6061 Al alloy sample. The treated and untreated samples were immersed in the solution separately and the weight loss was measured after 24 hours and 48 hours. The results of corrosion tests on some aluminum alloy samples are given in Table 4. Typical results for ion beam irradiated samples show a decrease in mass loss of up to 4 times. The ion beam treatment significantly increased the corrosion resistance of the treated Al samples surface compared to the untreated surfaces.

Sample	Weight Loss (mg / cm^2)			
	24 hrs.		48 hrs.	
	untreated	treated	untreated	treated
5083 Al	1.7	1.5	36.8	13.3
6061 Al	6.8	2.7	16.3	6.6

Table 4: Weight loss of some of the aluminum samples. A solution of 1% HCl was used for the 5083 and a solution of 5% NaCl and 0.3 H_2O_2 for the 6061 Al alloy sample.

DC anodic polarization measurements were done for treated samples of Al 6061 in a solution of 5% NaCl and 0.3 H_2O_2 and Al 2014 in 0.4% solution of HCl. The second electrode used in these measurements was graphite. The results of electrochemical measurements for Al 2014 and Al 6061 are given in Figure 21. The current amplitudes for the ion-treated samples compared to that for the untreated are a factor of 2.5 to 3 lower. This is also in reasonable agreement with the mass loss corrosion measurement.

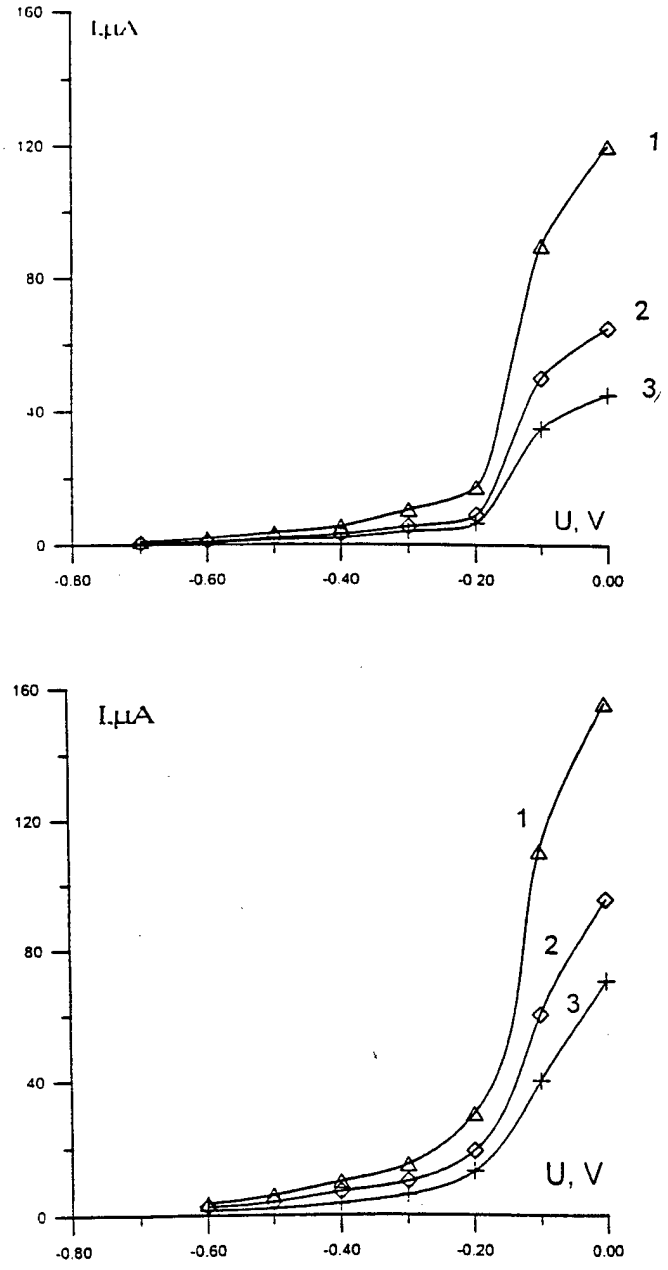

Figure 21: Anodic polarization curves for 6061 (upper) and 2014 aluminum (lower) alloys. Curve **1** is for untreated samples, curve **2** is for treated samples using 5 shots and a current density of 40 A/cm^2 and curve 3 is for treated samples using 5 shots at 70 A/cm^2 current density. The ion beam energy is 180 keV. The vertical axis is the measured current in microAmperes and the horizontal axis is the applied voltage in Volts.

Figure 22 shows the surface morphology of the 5083 Al alloy sample after corrosion in 1% HCl solution for 48 hours compared to the untreated side of the sample. It illustrates a pronounced improvement for the treated surface compared to the untreated one. This was typical for all the aluminum alloys that were treated with the ion beam.

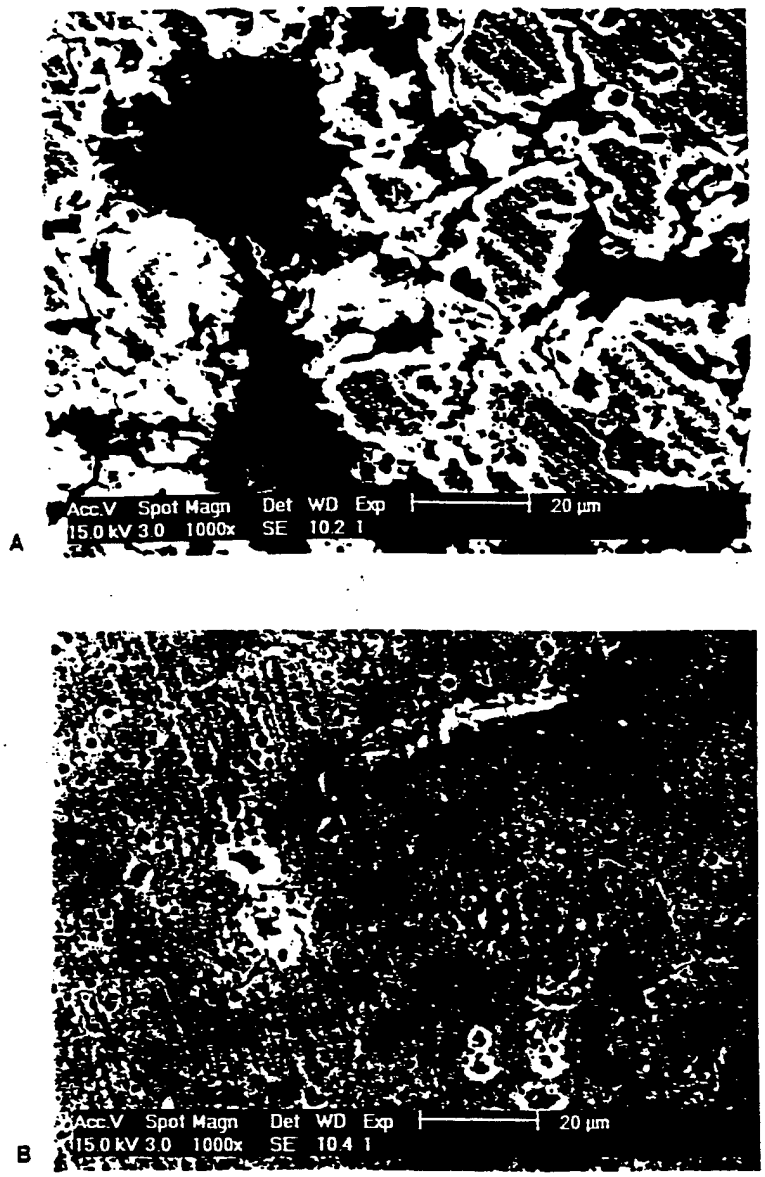

Figure 22: Optical micrograph of the surface microstructure of 5083 Al alloy corroded in 1% HCl for 48 hours. **A**--untreated surface, **B**--treated surface, the beam energy is 200 keV, and the current density is 100 A/cm^2.

Corrosion Tests on Irregular shaped Samples and Long Strips of Aluminum

As part of the Phase I effort we attempted to show that the ion beam treatment from our system is multidirectional in nature and not 'line of sight' as in vacuum ion diodes. Because the plasma density in our system is high enough to generate sheaths with thicknesses of a few mm we surmised that the ion beam, extracted from the plasma, would be capable of treating objects that are not flat but have surface irregularities on this scale. In order to demonstrate this we took 2014 aluminum alloy 5 mm thick and machined 'slots' of 2 mm depth into the surface (see Figure 6). The piece was masked so that one half was covered and would not be treated by the ion beam. The sample was mounted so that the flat 1 cm x 2 cm portion was held directly against the cathode surface. After treatment and corrosion for a 48 hour period, the sample was cut so that optical photographs could be made of the sides of the slots on both the treated and untreated regions of the sample. Figure 23 shows the results of this simple experiment. Note that the sides of the sample that were left exposed to the ion beam for treatment suffer much less corrosion than the untreated sides. Although this is not a particularly quantitative test, it is clear that the ion beam treatment can treat surfaces that are irregular in shape.

We also wanted to address the issue of sample size that could be treated by our system. Based on the current density as a function of position profile for our ion beam (see Figure 5) we decided to place a strip of 6061 aluminum about 10 cm in length on the cathode shank. The strip was held to the cathode with copper tape that was wrapped around it in three different locations. The copper tape prevents the ion beam treatment at these locations. After exposure to the ion beam we placed the strip in the 1% solution of HCl and left it for 48 hours. Figure 24 shows a photograph of the aluminum strip after corrosion. Note that the corroded 3 black bands are the locations where the copper tape held the Al strip to the cathode and were untreated.

Based on this simple test, an estimate of the surface area that can be treated for this system is ~ 250 cm^2. We have made this estimate by assuming that a 10 cm length can be treated over the

cathode surface of 8 cm diameter. This agrees with our assessment in the introduction which was based on the total ion beam current in our system. Note that we have only operated the system with 4 plasma guns during a shot. If we doubled the number of plasma guns then the length over which treatment could occur would effectively double and the treated area could be ~ 500 cm^2. Again, this test is not a particularly quantitative test, however it clearly demonstrates that reasonably large surface areas could be treated even with a system that is as compact as the one currently in use.

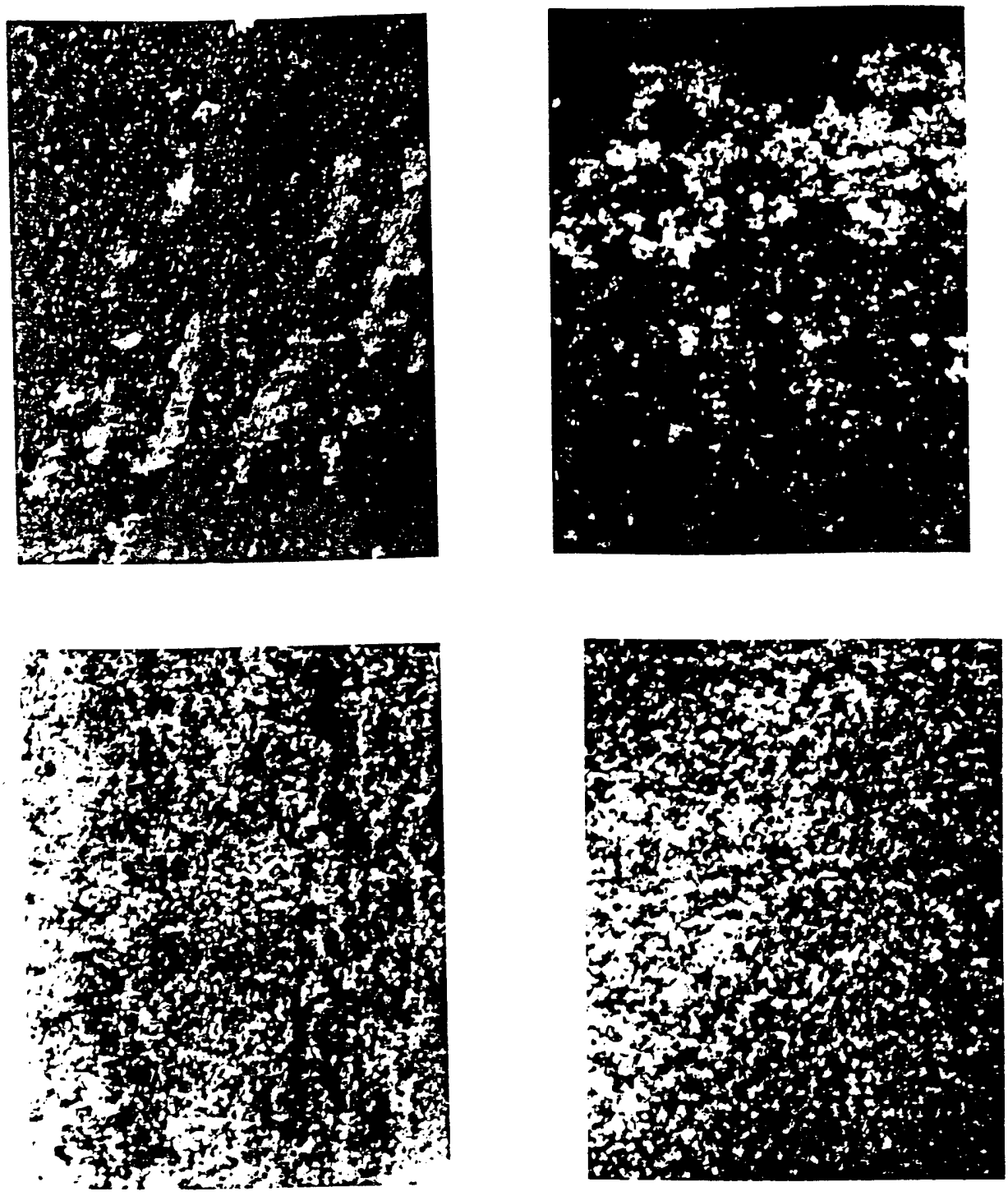

Figure 23: Optical micrographs of grooved aluminum 6061 after 48 hours in 1% HCl solution. The upper two photos show the side (upper left) and flat surface (upper right) of the untreated (masked) portion of the sample. The lower two photos show side (lower left) and flat surface (lower right) of the treated portion of the sample. The ion beam energy was 250 keV and the current density was 80 A/cm^2.

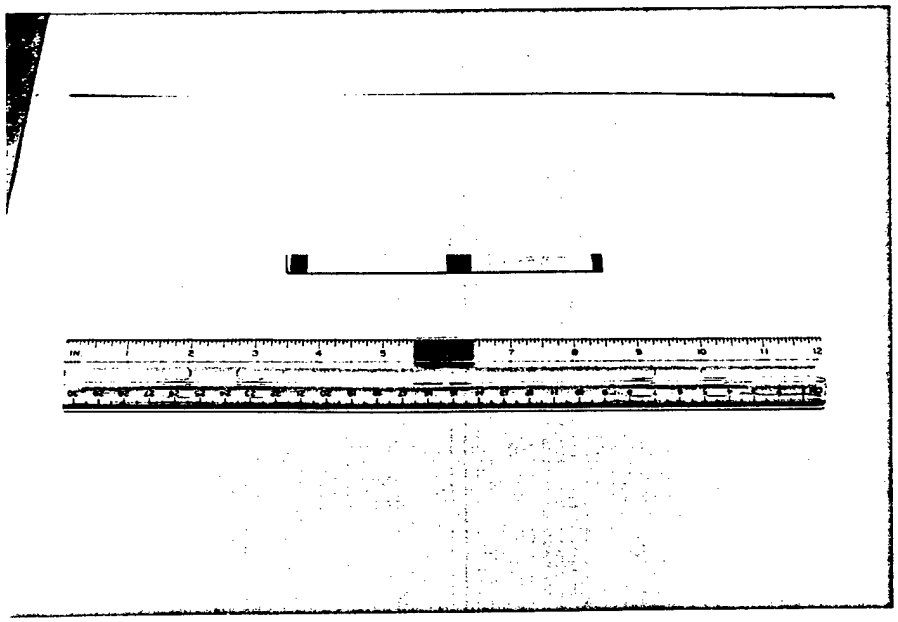

Figure 24: Photograph of the 10 cm long 6061 aluminum strip irradiated with a 250 keV, 100 A/cm^2 ion beam. The sample was placed in 1% HCl for 48 hours.

Samples With Pre-Deposited Thin Films

Single layer thin films of chromium, titanium or manganese were deposited on either carbon steel samples or aluminum samples. The films used in these studies were deposited using a four hearth electron beam evaporator. The carbon steel or aluminum 'substrates' were clamped 19" above the evaporation source and the deposition was monitored using a Leybold-Hereaus QC2000 Quartz Crystal Monitor (QCM) which was located 21.5" from the source. A shutter separates the source from the substrates. The thickness of the evaporated films were measured using a Tencor Alpha-Step 200 profilometer which also provided the calibration data for the

QCM. A typical scan on a 500 nm thick film is shown in Figure 25.

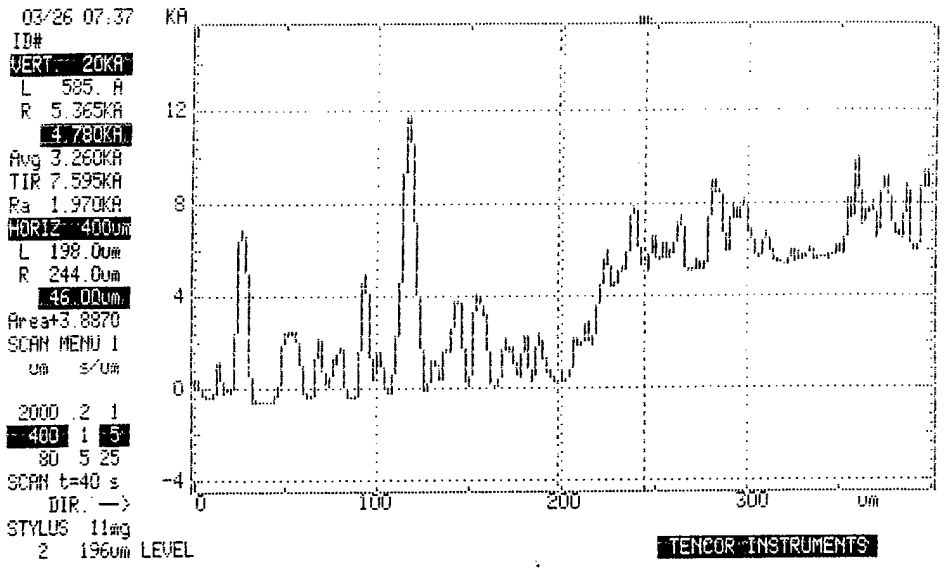

Figure 25: Profilometer scan of a thin film of chromium on a carbon steel substrate. The film thickness is about 500 nm.

The thin film layers we tried were either 160 nm, 300 nm or 500 nm in thickness. We tried these different film thicknesses because it was not clear whether the ion beam energy we had available in our system was sufficient to cause melting of the thin, deposited layer and the substrate underneath. During these experiments it became clear that there was not enough energy in the ion beam to melt the 500 nm thick chromium layer. This is one of the reasons we modified the system to generate higher energy density ion beams.

Characterization of the treated samples was done using the SEM, EDAX and Auger spectroscopy. The SEM analysis was sufficient to give us information on the surface morphology and whether it was likely that mixing occurred. If this appeared to be the situation then we performed EDAX on the sample. The EDAX analysis was done as a function of electron

beam energy for energies between 5 kV and 30kV, the maximum beam energy of the SEM. A comparison of the results of the EDAX analysis for treated and untreated parts of the same sample, as a function of electron beam energy, can give a qualitative picture of the composition of the sample as a function of depth since the electron beam range in the sample is a function of energy. The higher the electron beam energy, the longer the range in the sample and therefore, the deeper the sample is probed. We could plot percent composition of a given element, for both treated and untreated sides of the sample, versus electron range by estimating the range in the sample. A comparison of the plots was an indication of whether mixing occurred. If it seemed likely that the treatment caused some mixing then we had an Auger spectrum done.

We did not manage to get either the 300 nm or 500 nm chromium thin film layer to mix with either the steel or aluminum samples. SEM analysis of the surface showed that the chromium did melt to some depth but it was clear that no mixing occurred (Figure 26). We tried to irradiate the samples with different ion beam energies up to 250 keV and current densities of 180 A/cm^2. However, we could not find a suitable energy or beam current density that led to appreciable mixing, in fact it appears that a higher energy density is needed than the approximately 2.2 J/cm^2 our machine can deliver, or we can go to thinner films of chromium. Due to the time constraints of the program we could not do a very systematic study of the mixing as a function of beam energy and current density so we tried other combinations of thin film and substrate.

In the case of the manganese and aluminum substrate it appears that significant melting of the manganese thin film occurred but the manganese did not mix well with the aluminum. Instead, the manganese resolidified into small, less than several microns across, balls. Most likely this is due to the lack of solubility of manganese in the aluminum. Figure 27 shows an SEM of this phenomenon. EDAX on this sample, for different electron beam energies up to 30 kV, indicates that some mixing occurred but we did not try to quantify it due to the rather peculiar surface structure of the treated sample.

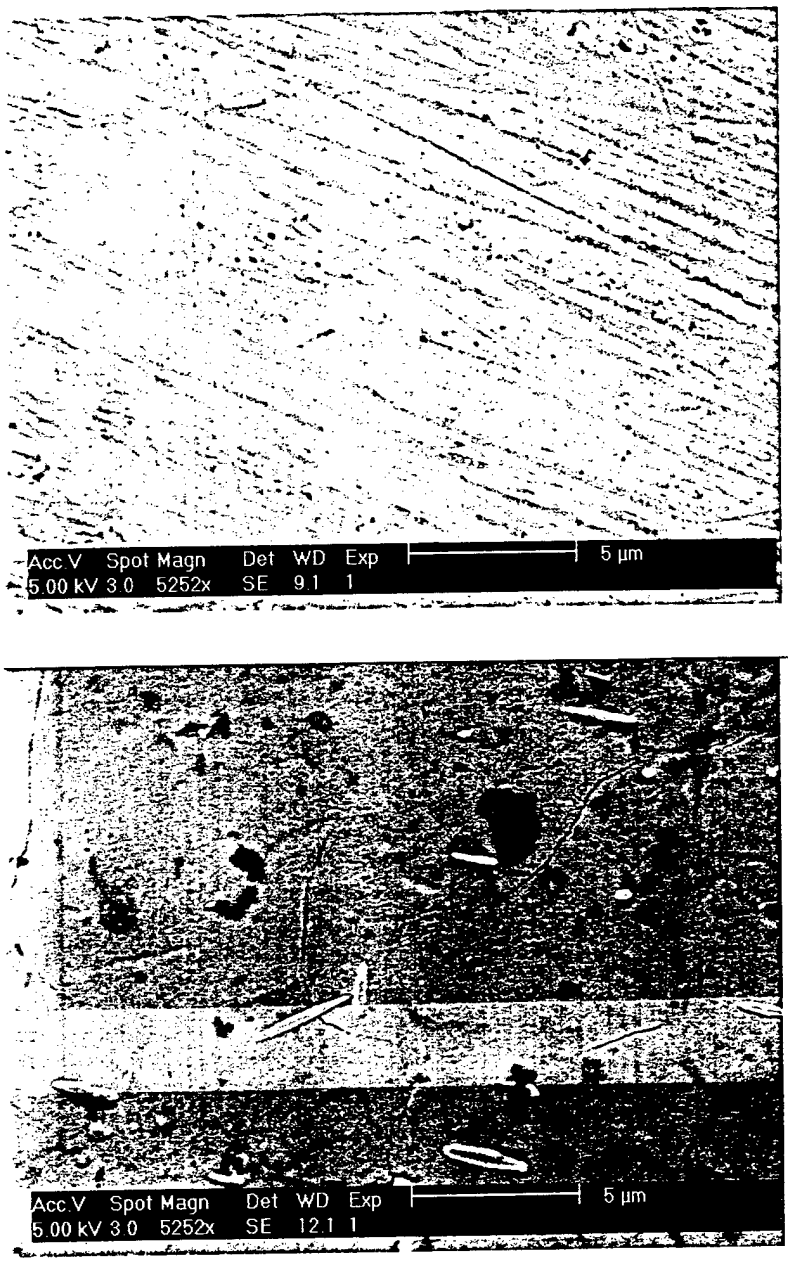

Figure 26: SEM of irradiated chromium thin film on a 1018 carbon steel substrate. The chromium film is 500 nm thick. Upper SEM is for the untreated portion of the sample. It appears as if surface smoothing occurs but no mixing. The ion beam energy is 250 keV and the current density is 150 A/cm^2.

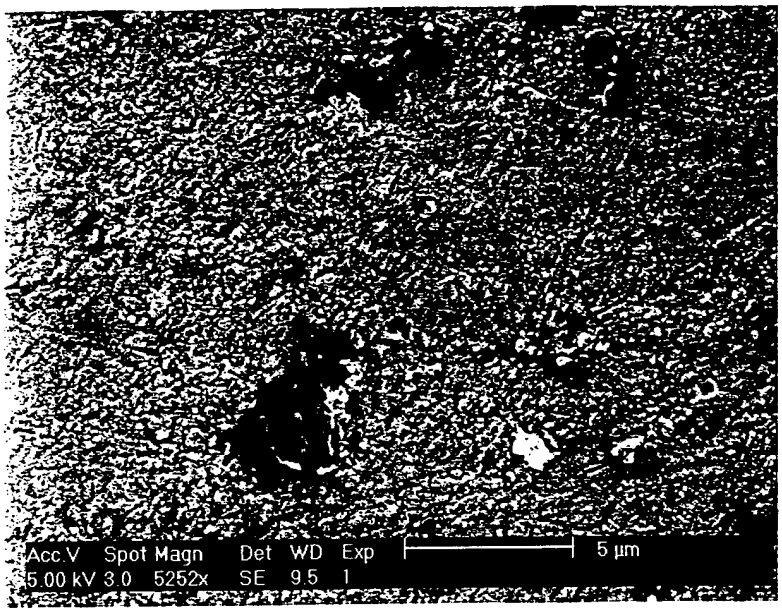

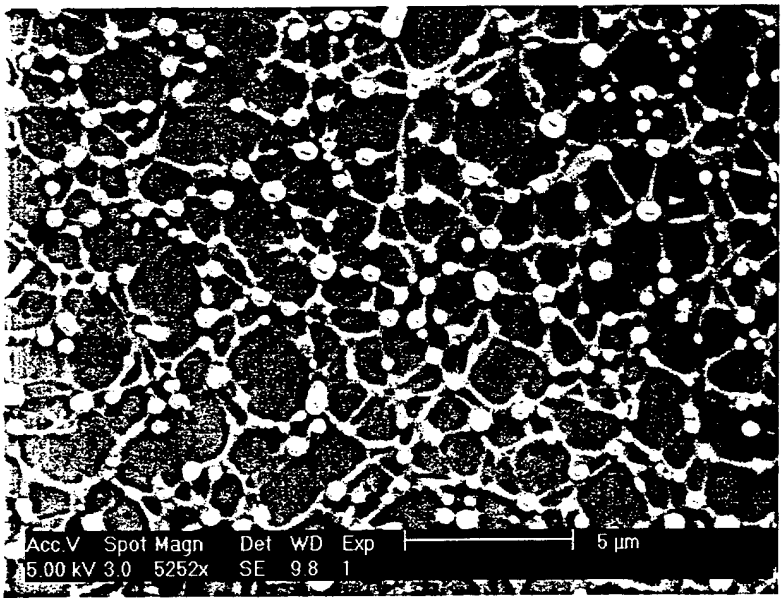

Figure 27: SEM of 160 nm thick manganese film on a 6061 aluminum substrate. The upper SEM is the portion that is not irradiated and the lower SEM is the irradiated portion of the sample. The ion beam energy is 250 keV and the current density is 150 A/cm^2.

The manganese film on carbon steel samples showed some mixing when we used a film thickness of 160 nm. For example, the EDAX analysis indicated that the untreated side of the sample had 40% manganese content when probed by a 30 kV electron beam and the treated side had about 10% manganese content when probed with the same beam energy. However, in the case of the manganese, the SEM analysis indicated that portions of the surface layer were evaporated so it is difficult to conclude, in detail, whether and how much of the manganese was mixed into the carbon steel substrate.

The best results we obtained in this work was on aluminum covered with a titanium film of 500 nm. We noted that the titanium layer was easy to 'peel' off the aluminum substrate before ion beam treatment. This seemed to be typical for our samples and may be due to improper preparation before film deposition, we are not sure. However, this observation gave us the opportunity to do some preliminary testing. We took an aluminum sample with the 500 nm titanium layer and treated the sample, masking, as usual, part of the sample so it would not be treated. We then put the sample in a 1% HCl solution. The titanium layer on the untreated side was 'bubbled' away, in a very short amount of time, by the corrosive action of the acid on the underlying aluminum. However, the treated side did not have the layer removed indicating a significantly better adhesion of the titanium film to the aluminum substrate for the treated side of the sample.

We also measured the microhardness of the aluminum substrate before deposition of the titanium film, after deposition and then after irradiation using the ion beam. The microhardness of the treated side of the sample was slightly lower than the untreated side of the sample. The microhardness of the aluminum substrate was about 50% lower than the treated or untreated part of the sample. Table 5 shows the results.

	6061	6061 and 500 nm Titanium film Untreated	6061 and 500 nm Titanium film Treated
Microhardness (HV)	110	160	155

Table 5: **Microhardness of titanium coated aluminum**. Microhardness measurements for the 6061 aluminum without titanium, with a 500 nm thick titanium layer and after treatment.

Figure 28 shows an SEM of the treated and untreated surface of the titanium covered aluminum substrate and Figures 29 and 30 give EDAX results on the untreated and treated parts of the sample, respectively. This particular result is for a probe electron beam energy of 10 kV. Note that the range of a 10 kV electron beam is barely sufficient to penetrate the 500 nm layer of titanium and so the untreated but coated area of the sample appears to be mostly titanium. EDAX at 5 kV indicated that the sample was titanium. EDAX analysis was carried out up to 30 kV for this particular sample. As a result of the EDAX, we had an Auger analysis done.

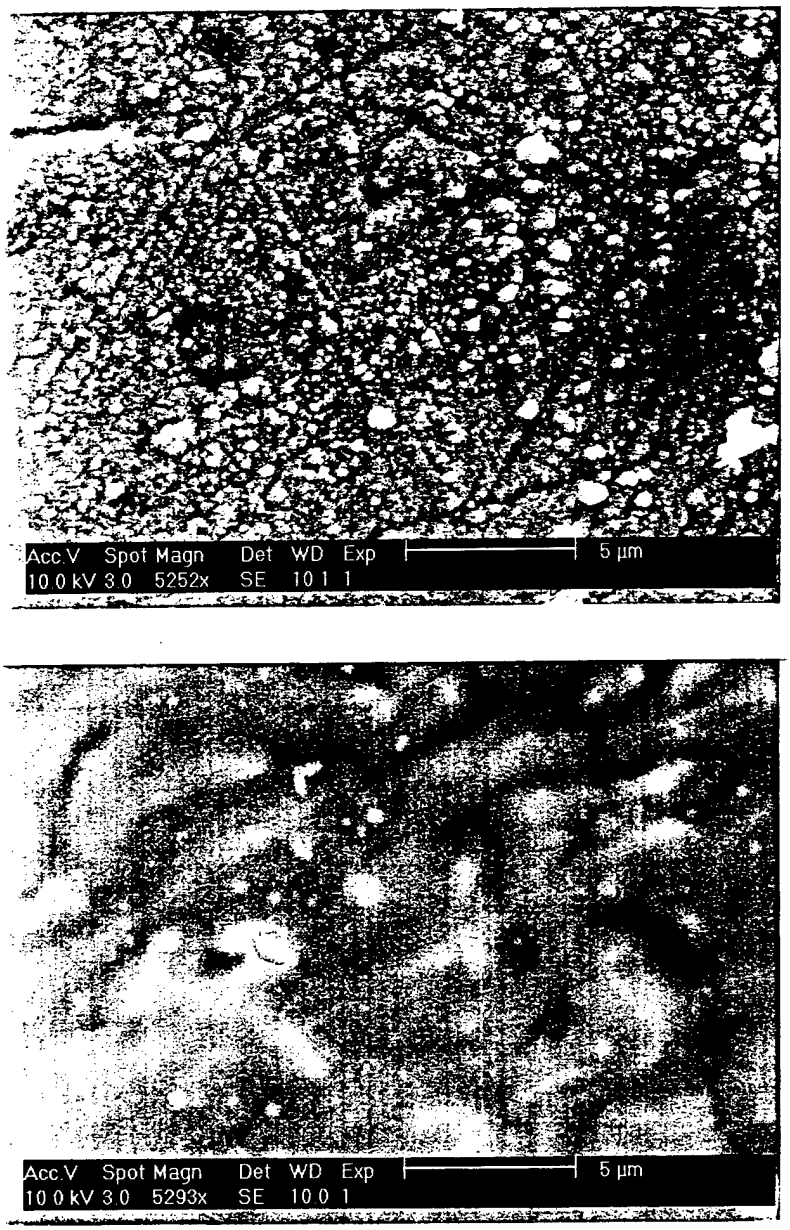

Figure 28: SEM of 6061 aluminum covered with a 500 nm thick film of titanium. The upper SEM is the untreated portion of the sample and the lower SEM is the treated portion of the sample. The ion beam energy is 250 keV and the current density is 150 A/cm^2.

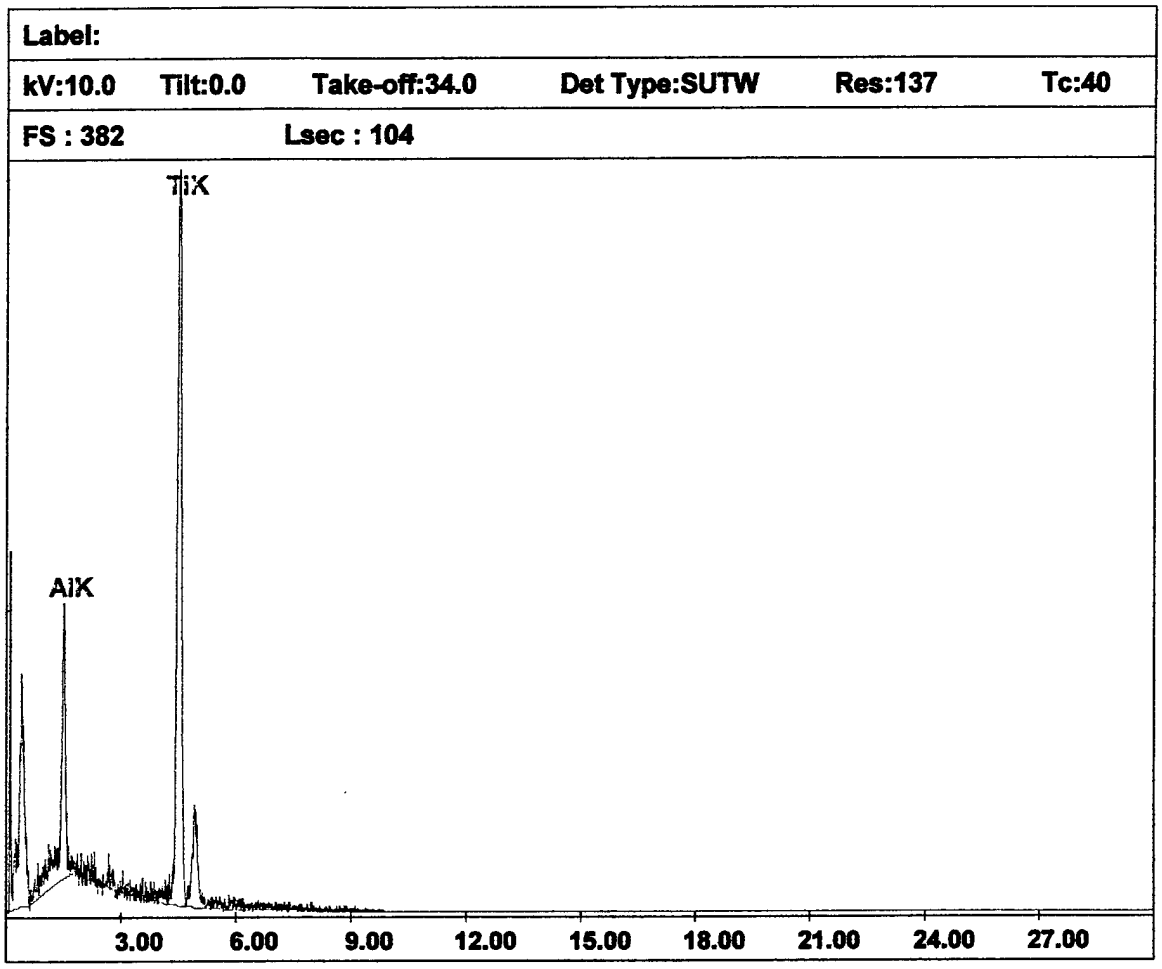

Element	Wt %	At %	K-Ratio	Z	A	F
AlK	6.41	10.84	0.0548	1.1110	0.7683	1.0012
TiK	93.59	89.16	0.9271	0.9918	0.9988	1.0000
Total	100.00	100.00				

Element	Net Inte.	Bkgd Inte.	Inte. Error	P/B
AlK	10.11	1.68	3.31	6.03
TiK	38.05	0.39	1.59	97.34

Figure 29: EDAX results at 10 kV for the untreated portion of the 6061 sample of Figure 28. At 5 kV electron beam energies the composition appears to be all titanium since the electron range in the titanium is less than 500 nm.

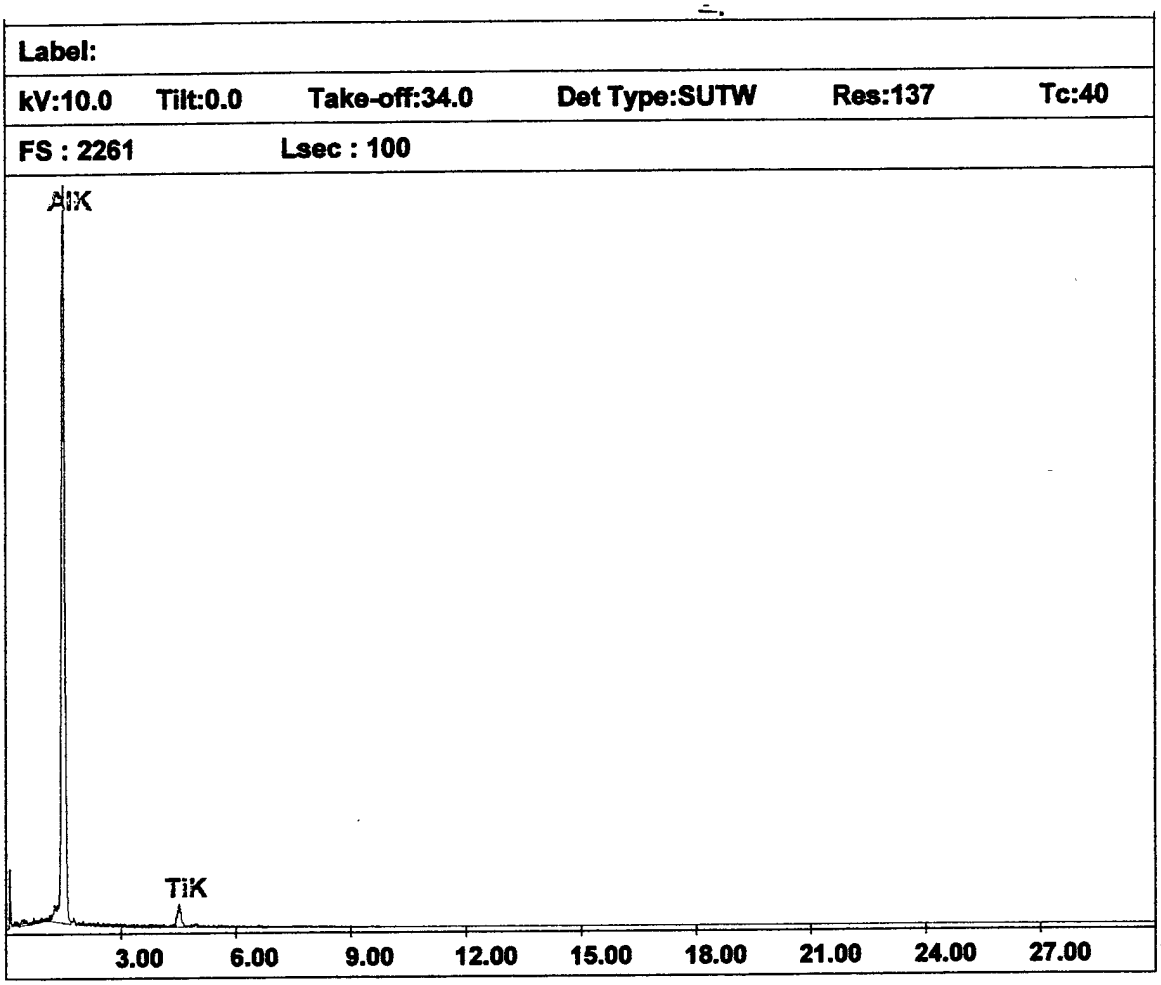

Element	Wt %	At %	K-Ratio	Z	A	F
AlK	84.59	90.69	0.8218	1.0160	0.9560	1.0003
TiK	15.41	9.31	0.1373	0.9050	0.9844	1.0000
Total	100.00	100.00				

Element	Net Inte.	Bkgd Inte.	Inte. Error	P/B
AlK	170.75	1.69	0.77	101.04
TiK	6.34	0.39	4.09	16.26

Figure 30: EDAX results at 10 kV for the treated portion of the 6061 sample of Figures 28 and 29. Additional EDAX at higher energies indicated that mixing of the titanium and aluminum likely occurred.

Figure 31 is the result of an Auger study on the treated side of the sample.

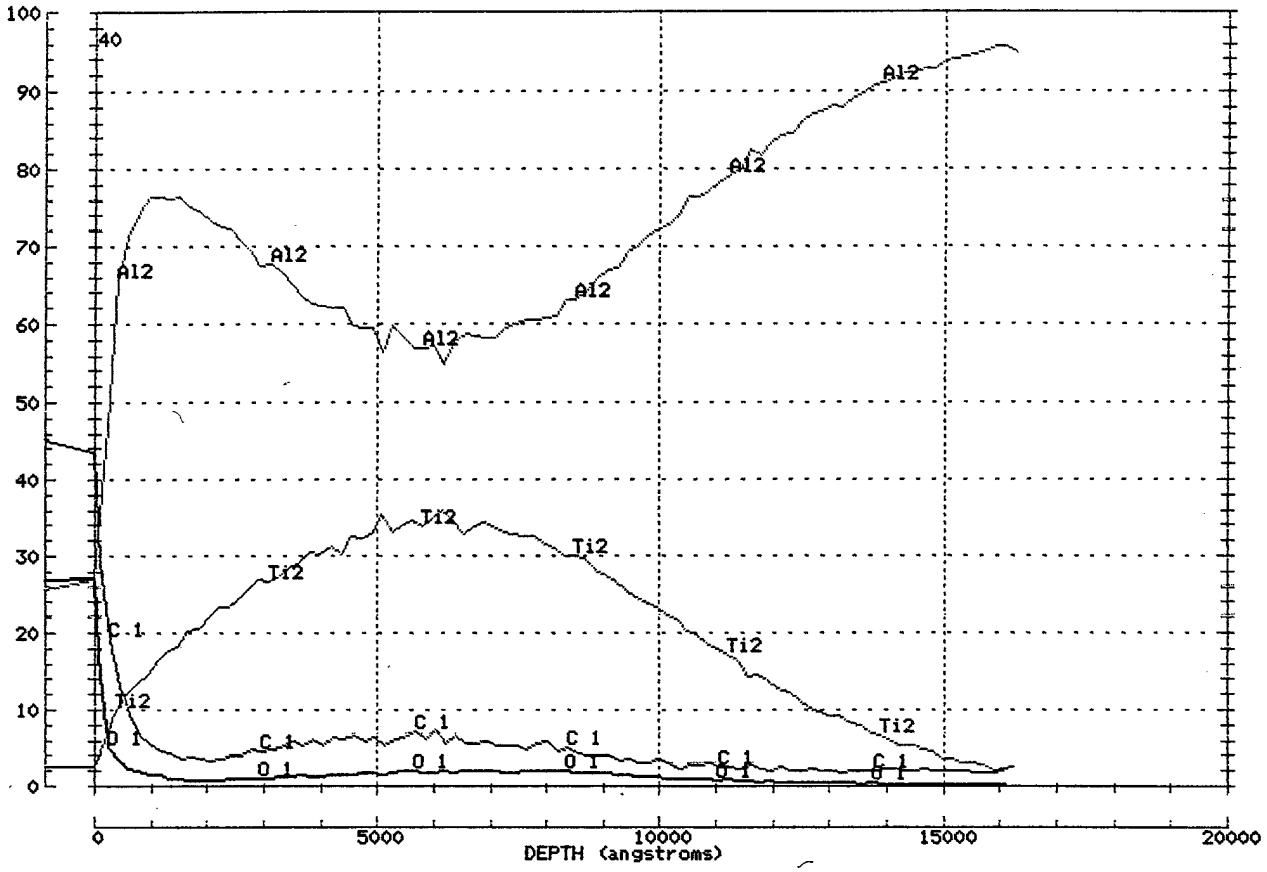

ACQUISITION PARAMETERS			
SPECTRUM TYPE:	AUGER PROFILE		
PRIMARY VOLTAGE:	5000	POINT NUMBER:	1
QUANTIFICATION TYPE:	Peak-Peak	QUANTIFICATION UNITS:	Atomic %

Figure 31: Auger profile of a 6061 aluminum substrate covered with a thin titanium film of 500 nm thickness after irradiation with a 200 keV, 150 A/cm^2 ion beam (sample of Figures 28-30). Significant mixing of the titanium occurs to depths of 1 micron. The carbon and oxygen are likely due to the plasma constituents and surface layers.

The Auger analysis was done as a function of depth by ion milling using an argon ion beam. The Auger was started after ion milling of about 500 Angstroms since there was surface contamination on the sample. Periodically during the Auger analysis, a 'profiling' of the composition of the sample was done since the Auger is carried out by setting the software to look for specific energies of electrons that correspond to elements. The Auger analysis looked for aluminum, titanium, carbon and oxygen. The periodic study of the composition showed that these were the most important constituents. Note that significant mixing of the titanium occurred even to depths of about 1 micron. Also, some carbon was found even to 0.5 micron. It is likely that this carbon results from the ion beam since the plasma constituents, from which the beam is generated, are carbon and hydrogen. The carbon seems to be mixed into the substrate, however, the amount is quite small. Oxygen also seems to be 'mixed' into the material, at quite small percentages. The oxygen is likely due to oxide layers on the surface before treatment. To the best of our knowledge these are the first results showing mixing due to ion beam irradiation in an MPOS system.

Future Work

There are three main areas of concern regarding this technology and its useful and commercial potential for surface modification of materials. These areas are: 1) Scale-up to system sizes compatible with commercial and military needs; 2) Construction of the system so that sample geometries other than cylindrical geometries can be treated and 3) System operation so that crater formation on the sample does not occur. We will briefly discuss these three concerns with the most important of these three areas of concern being the last, crater formation.

The Plasma Opening Switch (POS) has been under development in national laboratories and private companies throughout the world for the past 15 years [25-28]. The device is usually used as a power conditioning element on very high peak power pulsed systems. The purpose of the POS in these systems is to 'pulse compress,' i.e. convert 'long' pulses into much shorter ones and at higher voltages but without energy losses so that the peak power is increased. This is how our

system generates a 250 keV ion beam using a charging voltage of 45 kV. POS devices have been used on systems to generate greater than 5 MV and have been used on systems that conduct over 5 MegaAmpere of current. Greater than 1 kA/cm^2 ion beam current densities are easily generated. All of these systems exploit the same physical phenomenon, namely the magnetic cut-off of the electron current from the anode and the resulting rapid increase of the impedance of the plasma bridge. To provide the magnetic cut-off, a certain specific current density per unit length on the cathode surface is needed, which can be roughly estimated from the requirement that the magnetic field from this current is B_{self}=1 to 1.5 Tesla for magnetic insulation [22]. Therefore, for higher current amplitudes in the MPOS the size of the electrodes could be larger and the magnetic field would still be sufficient for cut-off. In our experiments the total area of the ion beam which was useful for treatment of surfaces was ~ 250 cm^2. By increasing the amplitude of the stored current 5 to 6 times we could use electrodes with much larger area. An additional benefit to this approach is that the efficiency increases for the ion current generation. The ion beam production efficiency is proportional to the total current amplitude carried in the plasma and for MA level currents the ion beam current could reach 60-80% of the total current stored in the MPOS. Also, MPOS devices have been operated in repetitively pulsed systems [29]. This could be an important factor in a production environment, although since only 3 to 5 shots seem necessary for effective surface treatment it is maybe not a major consideration. We think that the issue of scaling the system so that larger surface area parts can be treated is essentially straightforward. Scale-up requires more energy storage capability, roughly proportional to the increase in current, but this means either increasing the charging voltage (energy stored in the capacitor is proportional to charging voltage squared) or increasing the main storage capacitance. Scale-up permits higher energy density delivery to the sample surface. We think an MPOS system capable of delivering up to 10 J/cm^2 to the part could be straightforwardly constructed. Again, we would like to point out that scaling of the POS to large surface areas is a much more straightforward problem than that of scaling a vacuum ion beam diode so it could treat the same surface area.

The question of device geometry is somewhat less straightforward to address. Most of the development work on the POS has been done in cylindrical geometry. We have demonstrated in the Phase I effort that parts with nominally cylindrical geometry and surface irregularities, even on a few mm size scale, could be treated by our MPOS system. Parts like crankshafts, for example, have already been treated in previous work [10,11] at higher beam energies. The processing is straightforward due to the multi-directional nature of the ion beam and the small sheath thickness of the plasma. It is worthwhile to note that ion beams generated using vacuum diodes could not treat a surface like a crankshaft without implementing some mechanism to rotate the part, along two different axes, or sweep the ion beam.

Some work has been done on POS devices that are planar in geometry [24]. In this work the 'strip-line' was 14 cm in width and over 20 cm long. The system was configured to generate up to 200 kA of total current, yielding about 65 kA of ion beam current. Overall, the system size was similar to our MPOS, is as straightforward to construct as our system and the charging voltage was up to 50 kV, also similar to our device. Measured ion current densities were up to 150 A/cm^2. This work is important because it points out that an MPOS system could be easily constructed to treat flat surfaces and to generate high energy density ion beams. The part could also have surface irregularities on a mm scale that would also be treated since the plasma sheath in the planar geometry would be as small as in a cylindrical geometry device. If we assume that a flat part of aluminum is to be treated then, based on our Phase I effort, the current density needed would be about 100 A/cm^2. Assuming we configure a system to generate 200 kA of ion beam, which is not difficult, then a surface area of 2000 cm^2 could be treated. This will require an MPOS operating at a total stored current level of ~ 0.5 MA, which is only factor of 3 larger then the Phase I device. The main difficulty would be with plasma uniformity over the surface area. However, based on our Phase I results, aluminum can be treated with ion beam current densities that vary over a wide range of values, from 50 to 100 A/cm^2. Our results on Al corrosion show that the surface properties are not substantially different for treatment over this range of ion beam current densities. It is likely that treatment of flat panels of aluminum that are

50 cm on a side could be very straightforwardly implemented. The case for steels is different since the ion beam current density is an important consideration. It is also worth pointing out that very large flat surfaces could be treated by moving the part through the plasma-ion beam region. This would be an effective way to treat very large flat panels of any material.

The last issue that must be addressed for any of these 'thermal' ion beam treatments is crater formation on the surface of the treated material. The problem of crater formation occurs for vacuum ion diode systems and, as we discovered in our Phase I work, for devices like the MPOS. Our morphology studies indicate that craters can be up to 20 microns across, but are very shallow having depths of several microns. In addition, 'mounds' can form around the crater sights that have heights of 0.5 to 1.5 microns. It is not clear why the craters form in these ion beam (and pulsed electron beam treatments of material surfaces also show crater formation) treatments. There is likely a cause that is common to all these methods of treatment by charged particle beams and additional features specific to each method of treatment that exacerbates crater formation. For example, we could surmise that crater formation is due, in part, to the problem of boiling temperatures and their dependence on pressure. The melting temperature of aluminum is ~ 933 ^{0}K and the boiling temperature varies from ~ 2700 ^{0}K at 1 atmosphere to ~ 1750 ^{0}K at 1 Torr to 1060 ^{0}K at 10^{-6} Torr. So, if a pulsed ion beam heats the surface of aluminum to say 1200 ^{0}K and the background pressure is 10^{-4} Torr, then due to the development of melted surface convective instabilities, boiling could start at local points, like gas micro-bubbles, resulting in craters formation. The craters are then frozen into the surface during the rapid resolidification after the pulse. If this is correct then higher background pressures would actually aid in suppressing crater formation. It is worth pointing out that the MPOS works in relatively high background pressures, unlike vacuum ion diodes. The issue of background pressure would need to be further addressed in any continuation of this work.

It is worth noting that the above numbers are derived and measured for absolutely static conditions and their applicability for nanosecond transitional processes is more than

questionable. There is no data available in the literature relevant to nanosecond scale processes. It is also worth mentioning that if the suggested picture of crater formation is correct then the surface melting with any short pulsed driver (including melting under the action of powerful X-ray flow) will result in crater formation. However, recent results from experiments on surface modification using high power bursts of short pulsed X-rays (1 J/cm^2), indicate that craters did not form on the melted surface [30].

Taking this into account, it is more likely that crater formation could be related to formation of unipolar arcs between the plasma and local charged insulated patches at the sample surface (oil films, grease patches, absorbed gas, etc.) due to the incident charged particle flux. There has been some initial work on determining why crater formation is a problem for pulsed, charged beam treatment of materials, including the MPOS [31]. Besides the mechanism of crater formation discussed above, there are three other mechanisms that could be responsible for the crater formation: They are: 1) Explosive field emission. Because the sample is biased to negative high voltage during the ion beam irradiation, explosive field emission can occur on the sample at localities where the field is enhanced due to irregularities like whiskers. The electron emission heats the samples locally and plasma generation occurs at these 'hot spots'; 2) Formation of unipolar arcs near the cathode due to surface breakdown between insulated inclusions (gas, oil films, oxides) with formation of intense local micro-regions of dense plasma. This could also lead to formation of current microchannels between the plasma boundary and the cathode resulting in local surface overheating and formation of craters; 3) Bombardment of the cathode surface with microparticles ejected with the plasma flow from the erosion type plasma guns used in these systems.

These causes pertain to the quality of the primary plasma and conditions of the sample surface. Therefore active control of the plasma density and its uniformity could significantly improve the situation. The plasma can be generated in a number of ways that would prevent microparticles from being ejected into the area of the part to be treated. As an example, a gas type valve could be used to generate the plasma. We note that this type plasma source is now being tested by

Quantum Manufacturing Technology for their ion beam source. The previous plasma source they used was a surface flashover system much like the one we used to generate the plasma in our MPOS but, of course, much larger in size. Another possibility is to generate the plasma using cable type surface flashover guns, like we used in Phase I, but to place them in a magnetic filed with field lines that 'fringe' into the region where the part to be treated is located. The field can be generated using permanent magnets and only modest fields of several hundred Gauss are required. This type plasma source has already been used successfully in POS systems, but not for materials surface treatments. The plasma will follow the field lines into the treatment area but the ejected microparticles from the guns will be trapped out since they do not follow the field lines. Most likely an alternative to the surface flashover generation of the plasma is preferred, like the gas puff or even RF generation of a plasma in background gas, since it is cleaner and offers potentially more control of the plasma.

Also, considerable improvement of the situation could be provided with more thorough preparation of the cathode surface before the main pulse arrival. In the first stage we used only microsecond pre-treatment plasma pulses, at a low vacuum of 2 to 5 x 10^{-5} Torr, provided by a conventional oil diffusion pump. The pre-treatment stage could be prolonged by firing the plasma guns several times just before the main pulse, and / or by increasing the duration of the plasma pulse before firing the main pulse. The plasma can have an energy of up to 10 eV which should cause surface degreasing. Replacement of the oil diffusion pump with a turbomolecular pump would help by preventing backstreaming of oil into the system.

Another possibility is to heat the part which is to be modified. Experiments using samples heated to 300 ^{0}C and treated using an MPOS have been carried out for Sandia National Laboratory by the Tomsk ElectroPhysical Institute under contract number AM-2869. Results indicate that crater formation occurs only along surface irregularities like scratches. Perhaps this is due to a reduction in the number of centers that induce unipolar arc formation.

To conclude, we think the system is straightforwardly scalable so that larger surface areas can be treated. Also, MPOS systems can be configured to handle flat part geometries. Other part configurations can be handled in a cylindrical type MPOS geometry mainly because of the small plasma sheath and multidirectional character of the generated ion beam. However, the problem of crater formation, common to all pulsed, high power ion (or electron and laser) beam treatments of surfaces, will require a considerable part of the research effort in any Phase II program.

Other Work Done By Key Personnel of Applied Pulsed Power Technologies on MPOS Modification of Material Surfaces

Dr. Vitaly Bystritskii is PI and Dr. Eusebio Garate is Co-PI on a grant funded by DARPA under contract number F49620-96-1-0181 and awarded through the University of California, Irvine, to study the enhancement of corrosion resistance of aluminum alloys when irradiated by pulsed, high power ion beams using an MPOS. The MPOS system used for the DARPA studies is essentially the same as we have used in our Phase I work, however, we had to modify the MPOS to deliver higher energy densities for the various steel samples we studied in Phase I. The emphasis on the DARPA work is on corrosion resistance of aluminum alloys 6061, 2024 and 7075. The work also involves mechanical studies, on fatigue and stress, which compares the treated and untreated materials. The goal is to determine if 'bulk' properties change as a result of the ion beam irradiation. No work is being done under the DARPA award on irradiation of materials with pre-deposited surface layers and no work is being done on steels like M50, M2, D2 and some of the higher content carbon steels. The DARPA award is without a follow-on contract and does not involve scale-up of the system. The apparatus we use for all the DARPA work will treat small flat samples only. The question of crater formation does not seem to be of such concern for the DARPA technical contact. In fact, since the main goal is to increase corrosion resistance of these aluminum alloys, which are usually used in aircraft coated with primers and paint, it seems that perhaps the 'roughened' surface might actually improve adhesion of primers or paints.

References

1. Bystritskii, V.M., A.N. Didenko, High Power Ion Beams, APS, NY, 1990.

2. Stinnett, R.W., McIntyre, D.C., et al., Ion beam surface treatment: A new capability for surface enhancement, Proc. 10th Int. Conf. on High Power Particle Beams, 215, 1994, San Diego.

3. Stinnet, R.W., Buchheit, R.G., Rej, D.A., et al., Thermal surface treatment using intense, pulsed ion beams, in Mat. Res. Soc. Symp. Proc. Vol. 316, 521, R.J. Culbertson, O.W. Holland, K.S. Jones and K. Maex, editors, Symposium held Nov. 29 - Dec. 3, 1993, Boston, MA.

4. Buchheit, R.G., Maestas, L.M., Stinnet, R.W., et al., Pulsed ion beam surface treatment for preparing rapidly solidified corrosion resistant steel and aluminum surfaces, in Advances in Coating Technologies for Corrosion and Wear Resistant Coatings, A.R. Srivasta, C.R. Clayton and J.K. Hirvonen editors, TMS, 163, Warrendale, PA, 1995.

5. Olson, J.C., Davis, H.A., Rej, D.J., and Waganaar, W.J., Deposition and surface treatment with intense pulsed ion beams, Los Alamos National Laboratory Report LA-UR-95-570.

6. Rej, D. J., Microsecond pulse width intense light ion beam accelerator, Rev. Sci. Instrum, 64,(10), p. 2753, 1993.

7. Rej, D.J., Davis, H.A., et al., Plasma and Ion Beam Processing at Los Alamos, in Proc. 10th Int. Conf. on High Power Particle Beams, 222, June 20-24, 1994, San Diego, CA.

8. Wood, B.P., Rej, D.J., Davis, H.A., et al., Large-Scale implantation and deposition research at Los Alamos National Laboratory, Nucl. Instruments and Methods B-96, 429, (1995).

9. Rej, D.J., Gavrilov, N.V., et al., Carbon, nitrogen, and oxygen ion implantation of stainless steel, Los Alamos National Laboratory Report LA-UR 95-4148.

10. Bystritskii, V.M., S.V. Grigoriev, I.V. Lisitsyn, et al, Use of Microsecond Plasma Opening Switch for Material Surface Modification, Proc., 9th IEEE Conf. on Pulsed Power, Albuquerque, p. 1013, 1993. New Mexico.

11. Bystritskii, V.M., A.A. Sinebryukhov, V.A. Sinebryukhov, I. Lisitsyn, Application of Microsecond Plasma Opening Switch for Metal Surface Hardening, submitted to the Conference on Novel Applications of Lasers and Pulsed Power, part of the SPIE International Symposium on Photonics West '95, 4-10 February 1995, San Jose, CA.

12. Didenko, A.N., A.E. Ligachev, I.B. Kurakin, Influence of charged particle beams on metal and alloys surfaces, Moscow, Energoatomizdat, Moscow, 1987.

13. Shulov, V.A., G.E. Remnev, et al., Modification of materials properties by beams of charged particles, Proc. of All Russian Conference, v. 3, p. 3, 1991.

14. Hashimoto, Y., Yatsuzuka, M., Uchida, H., and Yamasaki, T., Metal surface characterization by intense pulsed ion beam irradiation, in 11th Int. Conf. on High Power Particle Beams, 848, Prague, June 10-14, 1996.

15. Remnev, G. E., Isakov, F., et al., Changes in the physical and mechanical properties of alloys exposed to high power ion beams, Proc. 10th Int. Conf. on High Power Particle Beams, 844, 1994, San Diego.

16. Vorobiev, O., Yu, Goel, B., Application of intense ion beams for investigation of matter properties under high pressure and temperatures, Proc. 10th Int. Conf. on High Power Particle Beams, 825, 1994, San Diego.

17. Remnev, G.E., and Struts, V.K., High power ion beam influence to stainless steels, in 11th Int. Conf. on High Power Particle Beams, 902, Prague, June 10-14, 1996.

18. Shulov, V.A., Nochovnaya, N.A., and Remnev, G.E., The application of high power ion beams in aircraft engine building for reconstruction of refractory alloy parts, in 11th Int. Conf. on High Power Particle Beams, 878, Prague, June 10-14, 1996.

19. Romanov, I.G., Tsareva, I.N., and Romanova, G.M., Influence of electron and ion beams of energy on the structural and mechanical properties of metals, in 11th Int. Conf. on High Power Particle Beams, 821, Prague, June 10-14, 1996.

20. Meli, C.A., Grabowski, K.S., Hinshelwood, D.D. et al., Film deposition and surface modification using intense pulsed ion beams, J. Vac. Sci. Tech. A, vol. 13(3), 1182, May/June 1995.

21. Bystritskii, V.M.; Mesyats, G.A.; Kim, A.A.; Koval'chuk, B.M.; and others. "Microsecond plasma opening switches," Fizika Elementarnykh Chastits i Atomnogo Yadra, Jan.-Feb. 1992, vol.23, (no.1):19-57. Translation: Soviet Journal of Particles and Nuclei, Jan.-Feb. 1992, vol.23, (no.1):7-24.

22. Bystritskii, V.M.; Lisitsyn, I.V.; Sinebryukhov, V.A.; Volkov, S.N., "Experimental studies of a microsecond plasma opening switch in the positive polarity regime with inductive load/extraction ion diode", Journal of Applied Physics, 15 June 1992, vol.71, (no.12):5772-82.

23. Bystritskii, V.M.; Bastrikov, A.N., et al., "Investigation of electron and ion flows in the microsecond plasma opening switch at teraWatt power level," IEEE International Conference on Plasma Science, pg 43, 22-24 May, 1989, Buffalo, N.Y.

24. Krasik, Ya. E., Arad, R., Weingarten, A., and Maron, Y., Energetic high current density electron/ion beam generation in plasma opening switches, in 11th Int. Conf. on High Power Particle Beams, 1039, Prague, June 10-14, 1996.

25. Goyer, J.R., Kortbawi, D., et al., Opening switch research and development for DECADE, Invited presentation, Proc. 10th Int. Conf. on High Power Particle Beams, 1, 1994, San Diego, CA.

26. Weber, B.V., Commiso, R.J., et al., Microsecond conduction plasma opening switch research at NRL, Proc. 10th Int. Conf. on High Power Particle Beams, 8, 1994, San Diego, CA.

27. Lisitsyn, I.V., Bystritskii, V.M., et al., Experiments with microsecond magnetically controlled plasma opening switch, Proc. 10th Int. Conf. on High Power Particle Beams, 17, 1994, San Diego, CA.

28. Savage, M.E., Hong, E.R., et al., Plasma opening switch experiments at Sandia National Laboratories, Proc. 10th Int. Conf. on High Power Particle Beams, 41, 1994, San Diego, CA.

29. Ushakov, A.G., Barinov, N.U., et al., Repetitive generators with plasma opening switch, Proc. 10th Int. Conf. on High Power Particle Beams, 21, 1994, San Diego, CA.

30. R. Baksht, Experiments on Material Surface Modification Using High Power X-ray Burst, private communication, Tomsk Institute of High Current Electronics, to be published.

31. see for example, Final Report to Sandia National Laboratory under contract AM-2869, from the Tomsk Electro-Physical Institute.